1. Title Page

Murine CMV infection unmasks macrophage-driven inflammatory cardiomyopathy in *Pkp2*, but not in *Ttn* mutant mice

Alexandra Cirnu, MSc[1,#], Tatjana Williams, PhD[1,#], Mike Nörpel, MD[1], Julian Kammerer[1], Svenja Kannt[1], Mairin Heil, MSc[1], Laura Kimmel, BSc[1], Anahi-Paula Arias-Loza, PhD[2], Manivel Lhoda, PhD[3,4], Thomas Henning, PhD[3,5], DiyaaElDin Ashour, PhD[6], Sarah-Lena Puhl, PhD[6], Giuseppe Rizzo, PhD[7], Clément Cochain, PhD[7,8], Tobias Krammer, PhD[9], Alexander Leipold, MSc[9,10], Antoine-Emmanuel Saliba, PhD[9,10], Matthias Mack, MD[11], Nicole Ziegler, PhD[12], Nancy Ernst, PhD[13], Ralf Joachim Ludwig, MD[13], Gustavo Campos Ramos, PhD[6,14], Stefan Frantz, MD[6,14], Lars Dölken, MD[3,5] and Brenda Gerull, MD[1,14,*]

[1]Comprehensive Heart Failure Center, Department of Cardiovascular Genetics, University Hospital Würzburg, Würzburg, Germany.

[2]Comprehensive Heart Failure Center, Department of Nuclear Medicine, University Hospital Würzburg, Würzburg, Germany.

[3]Institute for Virology and Immunobiology, University of Würzburg, Würzburg, Germany.

[4]The Rockefeller University, New York City, USA 10065.

[5]Institute of Virology, Hannover Medical School, Hannover, Germany.

[6]Comprehensive Heart Failure Center, Department for Translational Research, University Hospital Würzburg, Würzburg, Germany.

[7]Institute for Experimental Biomedicine, University Hospital Würzburg, Würzburg, Germany.

[8]Université Paris Cité, PARCC, INSERM, F-75015 Paris, France.

[9]Helmholtz Institute for RNA-based Infection Research (HIRI), Helmholtz-Centre for Infection Research (HZI), Würzburg, Germany.

[10]University of Würzburg, Faculty of Medicine, Institute of Molecular Infection Biology (IMIB), Würzburg, Germany.

[11]University Hospital Regensburg, Department Nephrology, Regensburg, Germany.

[12]Fraunhofer Institute for Translational Medicine and Pharmacology ITMP, Frankfurt am Main, Germany.

[13]Lübecker Institute for Experimental Dermatology LIED, Lübeck, Germany.
[14]Department of Internal Medicine I, University Hospital Würzburg, Würzburg, Germany.

[#]These authors contributed equally.

[*]**Correspondence to:** Brenda Gerull, MD. Email: Gerull_B@ukw.de. Comprehensive Heart Failure Center (CHFC) and Department of Medicine I, University Hospital Würzburg, Am Schwarzenberg 15, 97078 Würzburg, Germany.

Short Title: Murine CMV infection unmasks *Pkp2*-cardiomyopathy

Keywords: Genetic cardiomyopathy, PKP2, TTN, CMV, macrophages, inflammation

List of nonstandard abbreviations: ARVC/ACM – Arrhythmogenic right ventricular cardiomyopathy/Arrhythmogenic cardiomyopathy, PKP2 – plakophilin-2, DCM – Dilated cardiomyopathy, TTN – titin, MCMV – Murine cytomegalovirus, CCL2 – C-C motif chemokine ligand 2, CCR2 – C-C chemokine receptor type 2

Total Word Count: ca. 5600

2. Abstract

Background: Genetic cardiomyopathies display variable penetrance and phenotypic expression, highlighting the influence of environmental modulators. Myocarditis, commonly triggered by cardiotropic viruses, overlaps clinically with genetic cardiomyopathies. Consequently, these infections are implicated as secondary factors that accelerate disease onset and progression, yet their precise impact in specific genetic settings remains unexplored.

Methods: To interrogate this, genetic mouse models heterozygous for a mutant allele of desmosomal plakophilin-2 (*Pkp2*$^{+/-}$) or sarcomeric titin (*Ttn*$^{+/-}$), genes frequently linked to acute myocarditis, were challenged with murine cytomegalovirus (MCMV) to determine how latent infection influences myocardial inflammation, tissue remodeling, and cardiac performance. Integrated experimental approaches, including echocardiography, histology, flow cytometry, single-cell RNA sequencing, as well as cytokine and kinome analyses, defined immune and signaling responses in infected versus non-infected hearts.

Results: Acute, MCMV-induced viral myocarditis and subsequent latent MCMV infection unmasked early disease onset in *Pkp2*$^{+/-}$ animals, leading to progressive systolic impairment, whereas in *Ttn*$^{+/-}$ mice cardiac structure and function remained preserved throughout infection. Cardiac immune profiling uncovered infection- and genotype-specific divergence: both genetic models showed a stable myocardial effector-memory CD8^{+} T-cell response to MCMV, but only *Pkp2*$^{+/-}$ hearts recruited additional Ly6C^{+} CCR2^{+} monocytes and macrophages with distinct inflammatory signatures. In the absence of infection, *Pkp2* insufficiency initiated subclinical CCL2 secretion and subsequent recruitment of CCR2^{+} cells, reflecting early immune

activation preceding age-associated functional and structural decline. At this stage, cytokine and kinase evaluations indicated a balance between proinflammatory and compensatory signals. However, with aging or following MCMV challenge, this balance shifted towards persistent inflammation, evidenced by chronic upregulation of cytokines and activation of signaling pathways, which ultimately led to adverse effects and myocardial dysfunction.

Conclusions: Manifestation of genetic cardiomyopathies depends on interactions between inherited susceptibility and environmental stressors. Here, we show that cytomegalovirus infection intensifies inflammation in *PKP2*-related cardiomyopathy. In contrast, *TTN*-linked cardiomyopathy does not exhibit increased inflammation under the same conditions. For individuals carrying desmosomal variants, infection control and tailored anti-inflammatory strategies may attenuate or delay disease manifestation and progression.

3. Introduction

Clinical presentation and outcomes of patients with cardiomyopathies are determined by a combination of genetic and environmental factors. Among these, viral infections are thought to represent a contributing factor by initiating early cardiac damage and innate immune responses, leading to an acute stage of an inflammatory myopericardial syndrome (IMPS)[1]. Acute myocarditis-like episodes have been reported, especially in patients with arrhythmogenic right ventricular cardiomyopathy/arrhythmogenic cardiomyopathy (ARVC/ACM)[2]. Cardiotropic viruses, such as enterovirus, adenovirus and cytomegalovirus, have been detected in sporadic cases[3], suggesting a pathogenic link between ACM and viral infection. This has led to the hypothesis that pathogenic variants in desmosomal genes could increase the heart muscle's susceptibility to viral infections or inflammation. In this context, genetic alterations in desmoplakin (DSP) are frequently associated with myocarditis-like symptoms[2]; however, genetic variants in the most common disease-associated gene, plakophilin-2 (PKP2)[4], exhibit similar clinical features[5,6]. Heterozygous PKP2 variants show incomplete penetrance, resulting in a broad spectrum of phenotypes, ranging from patients with severe arrhythmias and heart failure to asymptomatic carriers[3]. As a result, the impact of non-genetic factors, especially viral infections, is gaining increasing importance. A recent meta-analysis revealed a high prevalence of pathogenic or likely pathogenic gene variants, notably in the sarcomeric gene titin (TTN) in addition to desmosomal genes (DSP, PKP2, and DSG2) among adults with myocarditis[7]. The presence of these gene variants coupled with acute myocarditis has been linked to a higher risk of adverse cardiovascular events, highlighting an essential connection between inflammation and accelerated disease progression in cardiomyopathies[8].

Titin truncating variants (TTNtv) are a common cause of dilated cardiomyopathy (DCM), accounting for up to 25% of cases[9]. Several modifying factors, including pregnancy, alcohol abuse, chemotherapy, and other comorbidities, contribute to overt disease[10]. Besides numerous human studies, we previously demonstrated that second hits like angiotensin II or isoproterenol led to the development of cardiomyopathy with cardiac dysfunction and fibrotic remodeling in a mouse model carrying an A-band Ttn truncating variant[11], however, the role of viral infections remains unknown, even though cardiotropic viruses have been detected in endomyocardial biopsies of DCM patients[12]. Animal models are therefore essential to dissect how secondary triggers interact with genetic susceptibility, shape immune activation and determine the timing of therapeutic interventions. Therefore, we aimed to study the mechanistic interplay among genetic predispositions, viral pathogenesis, and immune responses during infection with the common viral pathogen cytomegalovirus (CMV) in murine models of cardiomyopathy.

Human CMV infections generally remain subclinical in healthy individuals, but have been associated with cardiovascular diseases such as myocarditis. Additionally, seropositivity and lifelong latency are linked to a higher risk of developing inflammatory diseases later in life[13,14]. CMV can infect various cells in peripheral organs, including the heart, triggering typical immune responses involving innate and adaptive immune cells. Murine CMV (MCMV) closely resembles human CMV, mimicking its primary functional pathways, and is therefore used to study the acute and latent effects of viral infections on cardiovascular diseases[15].

Consequently, we examined the effects of MCMV infection as a second hit in two heterozygous genetic mouse models that mimic *PKP2*- and *TTN*-associated genetic predispositions. Interestingly, we observed distinct outcomes regarding the

88 development of cardiomyopathy and the role of the innate immune system in the
89 disease process. Heterozygous cardiac-restricted *Pkp2*$^{+/-}$ mice developed
90 progressive cardiac dysfunction linked to a myeloid cell and cytokine-driven
91 inflammatory response. In contrast, hearts of *Ttn*$^{+/-}$ mice remained unaffected despite
92 an appropriate MCMV-associated T-cell response. Furthermore, detailed age- and
93 time-dependent analyses of cardiac immune cell composition, cytokines, and their
94 receptors in *Pkp2*$^{+/-}$ mice indicate an early, intrinsic role for the CCL2-CCR2 axis and
95 suggest a potential therapeutic window for targeted inflammatory therapies.

4. Methods

All mouse studies and animal numbers used were in compliance with the Directive 2010/63/EU of the European Parliament, approved by the local ethics committee (RUF-55.2.2-2532-2-663, RUF-55.2.2-2532-2-962, and RUF-55.2.2-2532-2-1244) and conducted in accordance with the institutional guidelines.

Data Availability

A detailed methods section and all data supporting the findings of this study are provided within the article and its Supplemental Material. The RNA sequencing dataset is available from the NCBI Gene Expression Omnibus (GEO) under the GSE311777 accession number.

106 **5. Results**

107 **Cardiomyocyte-specific heterozygous loss of Pkp2 reveals normal myocardial**
108 **structure, function and immune cell composition**

109 To investigate how loss of one or both alleles of PKP2 affects cardiac structure,
110 function, myocardial inflammation and immune responses in a cardiac-specific
111 manner, we intercrossed *Pkp2* floxed mice with Cre-deleter mice in which the Cre
112 recombinase gene is expressed under the control of the α-myosin heavy chain
113 (αMHC) promoter which yielded homozygous (*Pkp2*$^{-/-}$, Figure 1A; S1A) and
114 heterozygous (*Pkp2*$^{+/-}$) knock-out mice. Homozygous loss of PKP2 protein (Figure
115 S1B+C) did not induce premature mortality, but caused marked biventricular
116 dysfunction at 6-8 weeks of age compared to age-matched control (Ctr) animals
117 (Figure 1B; Table S1). Consistent with this, picrosirius red (PSR) staining revealed
118 significantly increased collagen deposition in both ventricles (Figure 1C). However,
119 flow cytometry showed no differences in total CD45^{+} leukocytes,
120 monocytes/macrophages or infiltrating Ly6C^{+} monocytes compared to Ctr,
121 suggesting no active cell-based immune response at this already advanced stage of
122 disease (Figure 1D).

123 Since ACM is inherited in an autosomal dominant manner[16], we analyzed *Pkp2*$^{+/-}$
124 mice, which more closely reflect the human condition (Figure 1E). Consistent with
125 findings from other monoallelic desmosomal models[17-19], *Pkp2*$^{+/-}$ mice showed
126 structurally and functionally normal hearts at 9 months of age: left ventricular end-
127 diastolic diameter (LVEDD), left ventricular ejection fraction (LVEF) and tricuspid
128 annular plane systolic excursion (TAPSE) were preserved, while myocardial collagen
129 content or immune cell infiltration were not increased (Figure 1F-H; Table S2).

130

131 **MCMV infection causes progressive cardiac dysfunction in *Pkp2*$^{+/-}$ hearts**

132 The absence of an overt phenotype in *Pkp2*$^{+/-}$ mice provides an opportunity to
133 examine how viral triggers interact with genetic predisposition and cardiac immune
134 responses to potentially trigger disease. To assess this, 3-month-old *Pkp2*$^{+/-}$ and Ctr
135 mice were infected with 5x10^{5} plaque forming units (PFU) Δm157-MCMV-eGFP
136 (MCMV), a mutant strain that bypasses natural killer (NK) cell-mediated clearance in
137 C57BL/6J mice and ensures productive infection[20]. Mice of both genotypes received
138 phosphate-buffered saline (PBS) as a control (Figure 2A). Analyses covered time
139 points of acute (5-14 days post-infection, dpi), sub-acute (1-month post-infection,
140 mpi) and latent MCMV infection (3; 6mpi). Both infected genotypes developed
141 splenomegaly during acute infection, indicating immune system activation (Figure
142 2B). Hematoxylin-eosin (HE) and immunostaining revealed myocardial immune
143 infiltrates composed primarily of CD8^{+} T-cell plaques and scattered CD4^{+} T-cells in
144 either genotype during the acute phase (Figure 2C; Figure S2A). Quantitative PCR
145 for the viral *ie1* gene confirmed viral DNA persistence in heart, salivary gland and
146 lung with a gradual decline from acute to latent stages (Figure 2D; Figure S2B+C).
147 Serial echocardiography from 1 to 6mpi demonstrated a progressive decline in LVEF
148 exclusively in MCMV-infected *Pkp2*$^{+/-}$ mice as of 3mpi and worsening by 6mpi, while
149 LVEDD remained stable across all groups (Figure 2E; Table S3-S6). Collagen
150 content increased with age in all groups in a genotype- and infection-independent
151 manner (Figure 2F+G, Figure S2D-F). CD8^{+} T-cell numbers decreased from 1 to
152 6mpi in both infected genotypes, but remained higher than in non-infected hearts
153 (Figure 2H; Figure S2G; Table S7). Flow cytometry at 6mpi identified CD8^{+} KLRG1^{+}
154 terminally differentiated effector memory T-cells as the dominant expanded

155 population, consistent with MCMV-induced memory inflation in the $CD8^+$ T-cell
156 compartment[21]. Strikingly, monocytes/macrophages appeared more abundant in
157 *Pkp2*$^{+/-}$ MCMV than in Ctr MCMV hearts (Figure 2I, Figure S3). Together, these
158 findings show that while MCMV infection induces T-cell infiltration and persistent viral
159 DNA in both genotypes, *Pkp2*$^{+/-}$ MCMV mice selectively develop progressive systolic
160 dysfunction accompanied by monocyte/macrophage accumulation, establishing
161 MCMV as a potent trigger of cardiac disease onset in *Pkp2*$^{+/-}$ mice.

162 **CITE-seq and transcriptomic profiling reveal genotype-dependent and virus-**
163 **specific alterations of the cardiac immune compartment**

164 To define immune cell composition in chronically infected hearts, we performed
165 cellular indexing of transcriptomes and epitopes by sequencing (CITE-seq) of
166 ventricular $CD45^+$ leukocytes at 6mpi, excluding circulating cells by intravenous anti-
167 CD45.2-APC injection. Two independent experiments were performed, each
168 including 10 pooled samples (non-infected groups, n=2; MCMV groups, n=3), labeled
169 with TotalSeq-A hashtags that were used for demultiplexing (Figure 3A; Figure S4A;
170 Supplemental Methods). After quality control, doublet removal, and dataset
171 integration (Figure S4B), 26,656 cells remained for further analysis. Initial clustering
172 defined 16 immune cell groups that were annotated using canonical lineage markers
173 for T-cells (CD3, TCRβ), B cells (CD19), NK cells (NK1.1), neutrophils (Ly6G),
174 dendritic cells (CD11c), monocytes (Ly6C), and macrophages (CD64, CD88). Sub-
175 clustering of the lymphoid and myeloid compartments refined the annotation to 23
176 distinct populations, defined by combined transcriptomic and protein signatures
177 (Figure S5).

178 Dimensional reduction and compositional analyses revealed infection- and genotype-
179 dependent reshaping of the cardiac immune landscape. In both genotypes, latent
180 MCMV infection induced robust expansion of effector T-cell subsets, including
181 activated CD4^{+} Th1 cells (CD4_Th1_act; *Cd4, Cd28, Ctla4*), tissue-resident memory-
182 like CD8^{+} effectors (CD8_TRM_like; *Cd8a, Itga1, Gzmk, Klrc1*), terminal KLRG1^{+}
183 effector memory (CD8_Teff_KLRG1+; *CD8a, Klrg1, Gzmb, Ccl5*), and proliferating
184 CD8^{+} T cells (CD8_Teff_prolif; *Mki67, Top2a, Birc5*). Beyond this shared antiviral
185 response, *Pkp2*$^{+/-}$ MCMV hearts displayed a distinct myeloid signature with a marked
186 increase in cDC1 (*Xcr1, Clec9a, Itgae*) and antigen-presenting cDC2 cells (*Cd209a,*
187 *Bhlhe40, Dpp4*), as well as in two subsets of monocyte-derived macrophages. These
188 comprised a pro-inflammatory subset (moMac_Ly6C^{+}_inflam; *Plac8, Chil3, Ly6c2*)
189 and a reparative *Trem2*$^{+}$*Spp1*$^{+}$ subset (moMac_Trem2^{+}_Spp1^{+}; *Trem2, Spp1,*
190 *Fabp5*), the latter previously associated with profibrotic and tissue-remodeling
191 functions in the infarcted heart[22]. Interestingly, these subsets were already elevated
192 in non-infected *Pkp2*$^{+/-}$ myocardium compared to Ctr non-infected hearts, indicating
193 genotype-dependent priming of the myeloid compartment in the *Pkp2* heterozygous
194 setting (Figure 3B+C). No additional populations were selectively enriched in the
195 *Pkp2*$^{+/-}$ MCMV group, indicating convergence of viral and genetic factors on a
196 common immune response. To validate these compositional shifts, we performed
197 differential abundance testing using the MiloR framework, comparing *Pkp2*$^{+/-}$ non-
198 infected and *Pkp2*$^{+/-}$ MCMV hearts to Ctr non-infected mice, thereby allowing
199 assessment of genotype-dependent baseline changes and infection-driven
200 responses on the *Pkp2*$^{+/-}$ background. moMac_Ly6C+_inflam, cDC1, and cDC2
201 populations were significantly enriched when comparing non-infected *Pkp2*$^{+/-}$ and Ctr
202 hearts, confirming genotype-dependent expansion of myeloid subsets. Following

203 MCMV infection (*Pkp2*$^{+/-}$ MCMV vs. Ctr non-infected), CD8_TRM_like and
204 CD8_Teff_KLRG1+ populations overall displayed the strongest expansion, while the
205 underlying *Pkp2*-dependent myeloid alterations persisted (Figure 3D; Figure S6A).

206 To identify inflammatory mediators underlying these compositional changes, we
207 performed differential expression analysis of cytokines and their receptors across all
208 immune cell types (Figure 3E). Even in the absence of infection, non-infected *Pkp2*$^{+/-}$
209 hearts showed a distinct pro-inflammatory profile: *Ccr2* was strongly upregulated,
210 indicating enhanced recruitment and activation of monocytes and macrophages via
211 ligands like *Ccl2, Ccl7 or Ccl12*[23]. Elevated expression of *Il1b*, *Il1a,* and *Il6* further
212 supported activation of innate inflammatory pathways, while increased *Il17r* and
213 *Il17ra* indicated responsiveness to IL-17 signaling, typically associated with pro-
214 inflammatory Th17 cells[24]. In both genotypes, MCMV induced upregulation of *Ccl5*,
215 *Ifng* and its receptor *Ifngr1*, as well as *Il2rg* and *Il2rb*, components of the interleukin-2
216 receptor, implicated in regulating infection-associated T-cell responses[25,26]. In
217 addition, inhibitory molecules such as *Ctla4* were upregulated (Figure 3E). When
218 comparing *Pkp2*$^{+/-}$ MCMV to Ctr MCMV to isolate the genotype effect, a persistent
219 myeloid-dominant inflammatory signature emerged – again driven by *Ccr2* and
220 related mediators already identified in the *Pkp2*$^{+/-}$ non-infected hearts (Figure S6B).

221 Finally, pseudobulk differential expression was performed per cell type and subjected
222 to pathway enrichment analysis using the database MSigDB Hallmarks. In
223 Mac_TRM_MHCII+ macrophages, both comparisons (*Pkp2*$^{+/-}$ non-infected vs. Ctr
224 non-infected; *Pkp2*$^{+/-}$ MCMV vs. Ctr non-infected) revealed consistent enrichment of
225 immune activation pathways, with TNF-α signaling via NF-κB as the top hit.
226 Additional pathways included IL-6/JAK/STAT3 signaling, IL-2/STAT5 signaling and a
227 broad inflammatory response signature (Figure 3F, Figure S6C). Consistently, STAT3

228 protein levels were increased in infected and non-infected *Pkp2*$^{+/-}$ mice (Figure S6D).
229 Together, single-cell RNA and CITE-sequencing captured a subclinical accumulation
230 and activation of specific monocyte/macrophage populations already in
231 phenotypically unaffected non-infected *Pkp2*$^{+/-}$ mice, similar to those observed in
232 *Pkp2*$^{+/-}$ MCMV mice with systolic dysfunction. Therefore, the mutation itself already
233 reshapes the cardiac immune landscape. Nevertheless, an additional trigger is
234 required to actually cross the threshold for developing a clinical phenotype.

235 **The important role of the CCL2-CCR2 axis**

236 Next, we sought to identify soluble mediators that might attract or maintain
237 inflammatory cells in whole-heart protein samples and serum. This was done using
238 proximity extension assay-based proteomics at 6mpi (corresponding to 9 months of
239 age). Given the strong *Ccr2* upregulation observed in cardiac leukocytes, we
240 expected to identify one of its attractants *Ccl2, Ccl7* or *Ccl12*[23]. Interestingly, aside
241 from CCL2, several additional mediators were significantly upregulated in
242 phenotypically unaffected *Pkp2*$^{+/-}$ hearts (Figure 1E-H), including chemokines
243 involved in monocyte and macrophage recruitment (CCL2, CCL4, CXCL1), pro-
244 inflammatory cytokines (IL-1β) and immunoregulatory mediators (PD-L2, CCL22).
245 Additionally, the metabolic regulator FGF21 was increased and has been reported to
246 exert cardioprotective effects[27,28]. In contrast, these factors were not elevated in
247 serum. This cytokine response was amplified upon MCMV infection in *Pkp2*$^{+/-}$ mice:
248 in addition to FGF21, CCL2, CXCL1, CCL22, and CCL4, we observed upregulation
249 of CCL12 and CCL5. In serum, the most prominent change was a slight induction of
250 IL-6, consistent with systemic MCMV-driven inflammation, whereas heart-specific
251 mediators remained largely unchanged, indicating a predominantly local cardiac
252 response (Figure 4A; Figure S7A-C; Table S8+S9). Thus, these findings demonstrate

253 that *Pkp2*-deficiency alone is sufficient to elicit an early subclinical pro-inflammatory
254 milieu in the heart, consistent with recruitment of pro-inflammatory Ly6C^{+} CCR2^{+}
255 monocytes. Even though MCMV induced a CD8^{+} T-cell response, this was
256 associated with only a modest change in the overall cytokine spectrum compared
257 with the genotype-driven signals.

258 We next examined whether the expansion of myeloid populations in *Pkp2*$^{+/-}$ hearts
259 could be recapitulated using a macrophage-tailored flow cytometry panel. While in
260 *Pkp2*$^{+/-}$ MCMV hearts, Ly6C^{+} monocytes (typically also CCR2^{+}) and pro-inflammatory
261 macrophages (TIM4^{-}, MHC-II^{+}) were significantly increased, non-infected *Pkp2*$^{+/-}$
262 hearts, only showed a trend towards an increased abundance of these subsets
263 (Figure 4B+C), indicating that single-cell analysis is more sensitive at detecting an
264 early and cell-specific immune response. Together, these data show that *Pkp2*$^{+/-}$
265 hearts mount a local cytokine response amplified by MCMV, with recruitment of
266 Ly6C^{+} CCR2^{+} monocytes highlighting the CCL2/CCR2 axis as a central driver of
267 myocardial inflammation.

268 **MCMV infection in *Ttn*$^{+/-}$ mice does not induce cardiac dysfunction**

269 To test whether the combined effects of genetic predisposition and viral infection
270 reflect a broader principle in genetic cardiomyopathies, as observed in human
271 myocarditis patients[7], we applied the same experimental setup in mice with a
272 heterozygous global titin truncating mutation (*Ttn*$^{+/-}$), a model developing
273 cardiomyopathy under experimental stress conditions[11,29]. 9-month-old *Ttn*$^{+/-}$ mice
274 were indistinguishable from controls (Ctr), regarding cardiac function, collagen
275 deposition and immune cell abundance (Figure S8A–D). In accordance with the *Pkp2*
276 work, we infected 3-month-old *Ttn*$^{+/-}$ and Ctr mice with 5×10^{5} PFU MCMV and

277 performed analyses at 1, 3, and 6mpi (Figure 5A). Non-infected *Ttn*$^{+/-}$ and Ctr mice
278 received PBS and were combined into one control group. Echocardiography and
279 histology showed no genotype- or infection-dependent functional or structural
280 alterations at any time point following infection (Figure 5B+C; Figure S8E+F; Table
281 S10-S13). At 6mpi, immunostaining revealed scattered CD8^{+} T-cells in infected
282 hearts irrespective of genotype (Figure 5D). Flow cytometry confirmed infection-
283 induced expansion of cytotoxic CD8^{+} T-cells and KLRG1^{+} CD8^{+} T-cells in both
284 genotypes, with no change in monocyte/macrophage numbers (Figure 5E, Figure
285 S8G).

286 To capture subtle immune shifts, CITE-seq was performed on CD45^{+} cells at 6mpi
287 (10 hashed samples: Ctr non-inf n=2, *Ttn*$^{+/-}$ non-inf n=2, Ctr MCMV n=3, *Ttn*$^{+/-}$ MCMV
288 n=3; Figure S9A-C). Relative cell type abundance did not differ between non-infected
289 *Ttn*$^{+/-}$ and Ctr hearts, while both infected groups displayed expansion of activated T-
290 cell subsets (CD4_Th1_act, CD8_TRM_like, CD8_Teff_KLRG1+, CD8_Teff_prolif,
291 CD8_Tex_like; Figure 5F+G). Myeloid proportions remained unchanged across all
292 groups, in contrast to the genotype-driven myeloid skewing observed in *Pkp2*$^{+/-}$ mice.
293 MiloR[30] testing confirmed no differences between non-infected genotypes, justifying
294 their pooling in subsequent analyses. MCMV infection (*Ttn*$^{+/-}$ MCMV vs. Ctr non-
295 infected) enriched CD8_TRM_like, NK_eff, CD8_Teff_KLRG1+ and CD8_Tex_like
296 clusters, mirroring findings in Ctr MCMV hearts, while there was no difference
297 between both infected genotypes (Figure 5H; Figure S9D+E). Differential cytokine
298 expression analysis supported these results: *Ttn*$^{+/-}$ non-infected hearts showed no
299 upregulated inflammatory mediators, while MCMV infection induced *Ifng, Ccl5* and
300 IL-2 and IL-12 receptor components (*Il2rb, Il12rb2*) in both genotypes compared to
301 non-infected animals (Figure 5I, Figure S9F). Thus, in contrast to *Pkp2*$^{+/-}$ mice, *Ttn*$^{+/-}$

302 hearts exhibited no genotype-driven immune remodeling. All observed changes were
303 attributable to MCMV infection, underscoring the specificity of immune activation in
304 the *Pkp2*$^{+/-}$ model.

305

306 **Immune cell remodeling and phenotype development in aged *Pkp2*$^{+/-}$ mice**

307 To determine how inflammation, immune responses and cardiac function evolve with
308 age in the absence of viral infection, we longitudinally analyzed *Pkp2*$^{+/-}$ and Ctr mice
309 from 3 to 15 months of age (Figure 6A). Aging progressively reshapes the cardiac
310 immune landscape[31,32]. We thus hypothesized that interaction with *Pkp2* deficiency
311 might eventually unmask a cardiac phenotype.

312 Up to 9 months, *Pkp2*$^{+/-}$ mice maintained normal cardiac function despite a myeloid-
313 skewed inflammatory state (Figures 2E+3D+4A; *Pkp2*$^{+/-}$ non-infected at 6mpi). From
314 12 months onward, however, LVEF declined and LVEDD increased, progressing
315 further by 15 months, while Ctr hearts remained stable, indicating worsening systolic
316 function and ventricular remodeling (Figure 6B; Table S14+S15). Collagen content
317 increased with age in both genotypes but rose more steeply in *Pkp2*$^{+/-}$ hearts, with
318 fibrosis localized to the LV and RV endocardial layers (Figure 6C+D; Figure S10A).
319 Flow cytometry revealed progressive accumulation of inflammatory Ly6C^{+} monocytes
320 and persistently elevated total macrophages in *Pkp2*$^{+/-}$ hearts from 12 months
321 onward. Among macrophage subsets, pro-inflammatory antigen-presenting (TIM4^{-}
322 MHC-II^{+}) cells were consistently increased, despite an overall age-related decline in
323 this population (Figure 6E). Cytokine profiling supported these findings: IL-1β, CCL2
324 and CCL22 were elevated solely in *Pkp2*$^{+/-}$ hearts as of 9 months, while CCL12
325 increased only at 15 months, whereas none of these mediators were altered in

326 serum, indicating a localized rather than a systemic inflammatory response.
327 Cardioprotective FGF21 was already elevated in *Pkp2*$^{+/-}$ hearts as of 9 months and
328 additionally increased in serum at 15 months, suggesting an emerging compensatory
329 systemic response. In contrast, IL-10 remained unchanged in cardiac tissue but was
330 reduced in serum, consistent with a shift towards a pro-inflammatory milieu in *Pkp2*$^{+/-}$
331 mice (Figure 6F; Table S16+17). Together, these data show that physiological aging
332 unmasks systolic dysfunction, LV dilation, fibrosis and a sustained cardiac
333 inflammatory state in *Pkp2*$^{+/-}$ mice. Between 9 and 12 months, inflammatory markers
334 rise before the onset of overt fibrosis and contractile decline, defining a therapeutic
335 window during which anti-inflammatory intervention may attenuate immune activation
336 and fibrotic remodeling to preserve cardiac function.

337 To identify signaling networks associated with this early inflammatory state, kinome
338 profiling was performed in 12-month-old *Pkp2*$^{+/-}$ versus Ctr hearts. The significantly
339 regulated kinases were uniformly upregulated, indicating a coordinated activation of
340 inflammatory, immune, and compensatory signaling pathways (Figure 7A; Figure
341 S10B). IKBKE, PRKD1 and CSNK2A1 reflect activation and regulation of the NF-κB
342 pathway[33,34] sustaining chronic low-grade inflammation. FES, FGR, LCK and EPHA1
343 indicate enhanced immune-cell signaling and cell-cell communication, supporting the
344 immune activation observed at this stage. In parallel, MET, AKT3, PRKG1/2,
345 CSNK2A1 and RPS6KB2 suggest engagement of pro-survival and metabolic stress-
346 response pathways via PI3K-AKT-mTOR signaling[35]. STRING network analysis
347 showed connections between these immune-related and compensatory kinases
348 (Figure 7B), while KEGG pathway enrichment also reflected the dual activation of
349 different pro-inflammatory signaling pathways alongside pro-survival cascades,
350 indicating cardiac stress adaptation (Figure 7C). To assess whether kinase activation

351 translated into downstream pathway engagement at later stages, we analyzed hearts
352 from 15-month-old mice by Western blot (Figure 7D). Consistent with persistent NF-
353 κB activation, both total and phosphorylated p65 (p_i-p65) were increased in *Pkp2*$^{+/-}$
354 hearts compared with Ctr. These molecular changes coincide with the stage of
355 functional decline and fibrosis in aged *Pkp2*$^{+/-}$ hearts, confirming sustained NF-κB
356 signaling and chronic inflammatory stress.

357 **Early inflammatory signatures in homozygous *Pkp2*$^{-/-}$ hearts point towards**
358 **infiltrating monocytes as a therapeutic target**

359 The overall phenotype of heterozygous *Pkp2*$^{+/-}$ mice was moderate and became
360 apparent only upon the inflammatory trigger and at advanced age. To model a more
361 pronounced phenotype, we analyzed homozygous *Pkp2*$^{-/-}$ mice. Because 6-8-week-
362 old *Pkp2*$^{-/-}$ hearts already displayed extensive fibrosis (Figure 1C), mice were
363 examined at 3-4 weeks to capture earlier inflammatory stages (Figure 8A). However,
364 even at this age, echocardiography revealed functional impairment, albeit less
365 pronounced than at 6-8 weeks (Figure 8B). Interestingly, HE-stained hearts showed
366 clear immune cell accumulation between cardiomyocytes in both ventricles, which
367 stained positive for the macrophage marker CD68 (Figure 8C+D). Flow cytometry
368 confirmed significant infiltration of F4/80^{+} macrophages and Ly6C^{+} monocytes in
369 *Pkp2*$^{-/-}$ hearts. Sub-characterization revealed expansion of recruited pro-inflammatory
370 (TIM4^{-} MHC-II^{+}) and tissue-injury-associated macrophages (TIM4^{-} MHC-II^{-}),
371 alongside reduced tissue-resident macrophages (TIM4^{+} MHC-II^{-}), indicating a
372 monocyte-derived inflammatory response and identifying these cells as a potential
373 therapeutic target (Figure 8E). Cytokine analysis showed broad induction of
374 inflammatory mediators in *Pkp2*$^{-/-}$ hearts, including monocyte/macrophage
375 chemoattractants (CCL2, CCL12, CCL4, CCL22, CCL5), neutrophil chemokines

376 (CXCL1, CXCL2), eosinophil-recruiting CCL11 and pro-inflammatory cytokines (IL-
377 1α, IL-1β). Upregulation of immune checkpoints PD-L2 and CTLA4 suggested active
378 immunoregulation within the myocardium. These changes were largely heart-
379 restricted, with serum mediators mainly unaltered (Figure 8F). Recruitment of CCR2^{+}
380 monocytes via CCL2 and CCL12 thus represents a central feature of the *Pkp2*$^{-/-}$
381 model.

382 To examine whether this monocyte-driven inflammatory state can be modulated, we
383 treated 3-week-old *Pkp2*$^{-/-}$ and Ctr mice with an anti-CCR2 antibody (Figure 8G).
384 Treatment duration was limited to 7 days to prevent the formation of anti-drug
385 antibodies, which could compromise target engagement[36]. At the beginning of
386 treatment, mild fibrotic remodeling was already evident in *Pkp2*$^{-/-}$ hearts (Figure 8H).
387 Despite this, CCR2 blockade markedly reduced total cardiac
388 monocytes/macrophages, with similar trends toward decreases in Ly6C^{+} monocytes,
389 F4/80^{+} macrophages (Figure 8I), tissue-injury-associated and pro-inflammatory
390 subsets (Figure S11A+B), confirming the monocytic origin of the likely disease-driving
391 myeloid populations in this model. Fibrosis and cardiac function remained unchanged
392 due to the short treatment period (data not shown). These data confirm effective
393 depletion of CCR2^{+} myeloid populations *in vivo* and indicate that the cellular and
394 tissue state at treatment onset likely shapes the measurable downstream effects.

395 Across genetic, viral and aging models, our data show that, in particular, the *Pkp2*$^{+/-}$
396 genotype and therefore disturbed desmosomal proteins predispose to immune
397 remodeling that accelerates with secondary stressors, whereas complete loss of
398 *Pkp2* rapidly triggers monocyte-driven inflammation and cardiac dysfunction,
399 highlighting inflammatory monocytes as a therapeutic target population.

6. Discussion

In this study, we demonstrate that murine cytomegalovirus (MCMV) infection acts as a potent, genotype-dependent environmental modifier, unmasking early disease in phenotypically unaffected cardiac-restricted *Pkp2*$^{+/-}$ mice, but not in *Ttn*$^{+/-}$ mice. While both models exhibited persistent effector-memory CD8^{+} T-cells in the myocardium during latent infection, only *Pkp2*$^{+/-}$ MCMV mice developed progressive systolic dysfunction accompanied by increased recruitment of monocytes and macrophages - findings that were absent in *Ttn*$^{+/-}$ MCMV mice. These results reveal that MCMV does not trigger a generic response in genetic cardiomyopathies, but instead amplifies desmosome-related inflammation, driving ACM-like pathology. Even in the absence of infection, the *Pkp2*$^{+/-}$ genotype alone induced a subclinical pro-inflammatory state, which is mediated by the CCL2/CCR2 signaling pathway. With aging, *Pkp2*$^{+/-}$ mice developed fibrosis and overt contractile dysfunction in the absence of MCMV, marking a transition from compensated inflammation to pathological remodeling. Together, these findings establish viral infection as a disease-modifying factor in ACM, delineate mutation-specific inflammatory mechanisms distinguishing ACM from other cardiomyopathies, and identify the subclinical inflammatory phase as a promising therapeutic window for anti-inflammatory intervention.

As a cardiotropic virus with high seroprevalence in the human population, CMV establishes lifelong latency and can reactivate, for instance, under inflammatory stress[37,38]. MCMV closely mirrors the human infection, reproducing key virological and immunological features, including reshaping of the T-cell compartment through memory inflation, which maintains chronic low-grade inflammation[21]. To prevent rapid NK cell-mediated clearance typical for wild-type MCMV in C57BL/6 mice, we used a

424 m157-deficient strain (Δm157-MCMV-eGFP) that bypasses recognition by the
425 activating NK cell receptor Ly49H and shifts the antiviral defense toward a sustained
426 $CD8^+$ T-cell response[20,39]. Consistently, we observed prominent $CD8^+$ T-cell plaques
427 in acutely infected hearts that declined but persisted up to 6mpi. A subset of these
428 cells expressed KLRG1, indicating an effector-memory phenotype characteristic of
429 CMV-driven memory inflation and a chronic pro-inflammatory milieu[40]. Importantly,
430 Ctr MCMV mice in both genetic models did not develop systolic dysfunction or
431 fibrosis, reflecting asymptomatic latent infection in immunocompetent hosts. In
432 contrast, *Pkp2*$^{+/-}$ mice with latent MCMV infection developed progressive systolic
433 dysfunction without structural remodeling, establishing MCMV as a potent second hit
434 that unmasks disease in a genetically primed background. Infection amplified the pre-
435 existing inflammatory state in *Pkp2*$^{+/-}$ mice, marked by early cytokine activation and
436 myeloid cell recruitment. At the same time, additional $CD8^+$ T-cell infiltration further
437 enhanced cytokine signaling and was associated with functional decline. Previous
438 studies have shown that chronic inflammatory mediators can exert negative inotropic
439 effects[41] and destabilize desmosomal integrity[42], thereby impairing cardiac
440 contractility, providing a possible explanation for the observed phenotype in our
441 model. However, this MCMV-induced phenotype was genotype-specific. *Ttn*$^{+/-}$ mice
442 carrying a truncating titin variant[11], despite mounting a similar $CD8^+$ T-cell response,
443 showed preserved cardiac function and no signs of additional inflammation
444 throughout the entire time course. Previous studies demonstrated that stimulation
445 with angiotensin II or isoproterenol induced systolic failure and fibrosis in
446 phenotypically silent *Ttn*$^{+/-}$ mice, indicating that the described pathology is linked to
447 biomechanical rather than inflammatory stress[11,29]. Thus, the mechanisms by which
448 *Pkp2* and *Ttn* mutations lead to cardiomyopathy diverge: desmosomal disruption

generates an intrinsic pro-inflammatory state that viral infection can amplify, whereas titin mutation-driven disease appears to be dominated by stress-responsive or possibly autoimmune mechanisms. Together, these findings establish CMV as a context-dependent modifier of genetic cardiomyopathy in mice, revealing that viral infection amplifies mutation-specific immune mechanisms rather than acting as a universal pathogenic trigger across genotypes and model systems.

In the absence of external triggers, *Pkp2*$^{+/-}$ mice exhibited a slowly progressive phenotype that mirrors the clinical trajectory of ACM, transitioning from a concealed phase to overt cardiac dysfunction. Cardiac function remained preserved up to 9 months of age, followed by the onset of interstitial fibrosis and contractile impairment from 12 months onward. Molecularly, this progression was preceded by early upregulation of CCL2, a chemoattractant for cells expressing its receptor CCR2, along with increased IL-1β signaling in *Pkp2*$^{+/-}$ hearts. These changes promoted the recruitment of Ly6C^{+} CCR2^{+} monocytes and, ultimately, pro-inflammatory macrophages. These events parallel findings in *Dsg2*-based ACM models, where *Ccl2/Ccr2* upregulation and macrophage influx were identified as an early sign of the disease process[18,43]. In addition, we identified *Trem2*$^{+}$*Spp1*$^{+}$ macrophages resembling the reparative *Trem2*^{hi}*Spp1*^{hi} population described after myocardial infarction (MI)[44]. Unlike the sequential inflammatory-to-reparative transition seen after MI, Ly6C^{+} CCR2^{+} monocytes and *Trem2*$^{+}$*Spp1*$^{+}$ macrophages coexisted in *Pkp2*$^{+/-}$ hearts, indicating persistent low-grade signaling that sustains both inflammatory and pro-fibrotic programs. In a model of acute viral myocarditis, *Spp1*$^{+}$ macrophages instead adopted a pro-inflammatory role by inducing fibroblast *Ccl2/Ccl7* expression and promoting CCR2^{+} cell recruitment[45]. These findings highlight the environment-dependent heterogeneity of macrophage function in acute and chronic settings. At 9

474 months, apart from pro-inflammatory molecules, several immunoregulatory mediators
475 were elevated, including CCL22, which attracts regulatory T cells[46]; PD-L2, a ligand
476 of the PD-1 checkpoint receptor that dampens T-cell activation[47]; and FGF21, a
477 cytokine with cardioprotective effects in mice limiting cardiac damage in hypertension
478 and oxidative stress[27,28]. These changes suggest an early balance between pro- and
479 anti-inflammatory signals. With age, this equilibrium shifted toward chronic
480 inflammation, reflected by CCL12 expression at 15 months and also in *Pkp2*$^{+/-}$ MCMV
481 hearts at 6mpi. A similar *Ccl12* induction has been reported in *Dsg2*^{cKO} mice during
482 late stages of disease, consistent with a shared inflammatory program driving CCR2^{+}
483 cell recruitment[43]. Moreover, in the setting of MI combined with chronic periodontal
484 inflammation, *Ccl12* was shown to prolong inflammation and impair cardiac wound
485 healing, underscoring its role in sustaining maladaptive immune responses[48]. Kinome
486 profiling at 12 months revealed concurrent activation of immune-cell kinase networks
487 and stress-response pathways. Upregulated kinases included IKBKE and PRKD1,
488 both activators of NF-κB[33,34], and FGR, FES and LCK, linked to myeloid and
489 lymphoid signaling[49-51], together indicating sustained innate immune activation.
490 Correspondingly, phosphorylated p65 and total p65 were elevated in 15-month-old
491 *Pkp2*$^{+/-}$ hearts, confirming persistent NF-κB activity. While NF-κB-mediated monocyte
492 recruitment has been described in *Dsg2*$^{mut/mut}$ models[52], our data extend this
493 mechanism to heterozygous *Pkp2* deficiency. Interestingly, Pérez-Hernández et al.
494 also identified NF-κB as a transcription factor associated with PKP2, implying that
495 PKP2 deficiency makes cardiomyocytes more prone to sterile myocarditis, which can
496 be worsened by inflammatory or viral triggers[53], as shown in our study. Integrating
497 these findings, we propose that the *Pkp2*$^{+/-}$ genotype intrinsically activates NF-κB-
498 dependent signaling in cardiomyocytes, driving sustained release of CCL2 and, at

499 later stages, CCL12. This chemokine profile promotes recruitment of CCR2^{+}
500 monocytes and impairs resolution of inflammation, resulting in the persistence of
501 macrophages with both inflammatory and pro-fibrotic properties. Such inflammatory
502 activation was absent in *Ttn*$^{+/-}$ hearts, underscoring the genotype-specific nature of
503 this response. In *Pkp2*$^{+/-}$ hearts, sustained macrophage activity likely drives
504 progressive injury by releasing proteases and reactive oxygen species[54], which
505 promote extracellular matrix remodeling and systolic dysfunction. Identifying this
506 inflammatory phase before irreversible fibrosis develops defines a promising window
507 for therapeutic intervention.

508 Building on this CCR2-centered mechanism, studies in *Dsg2*$^{mut/mut}$-based ACM have
509 demonstrated that genetically blocking CCR2-dependent monocyte recruitment
510 reduces macrophage-driven fibrosis[52], supporting the idea that CCR2^{+} cells directly
511 contribute to desmosomal injury. In our *Pkp2*$^{-/-}$ model, CCR2^{+} macrophages were
512 similarly the predominant expanded population, and short-term anti-CCR2 treatment
513 showed effective depletion *in vivo*. Even though the intervention was initiated when
514 fibrotic changes were already present, the reduction in CCR2^{+} myeloid cells suggests
515 that blocking this pathway at an earlier, inflammation-dominated stage would
516 probably exert a more pronounced effect - consistent with findings from the
517 *Dsg2*$^{mut/mut}$ studies. However, sustained depletion of CCR2^{+} cells is not feasible in
518 human patients because of their critical role in immune defense. Thus, although
519 CCR2^{+} monocytes represent a shared disease-driving population across
520 desmosomal cardiomyopathy models, these findings suggest that precisely timed
521 modulation of early inflammatory signaling, rather than global depletion of myeloid
522 cells, is the more promising therapeutic strategy.

523 Currently, no approved disease-specific targeted therapy exists for ACM, and anti-
524 inflammatory or immunosuppressive agents such as glucocorticoids (e.g.,
525 dexamethasone) and azathioprine are used only occasionally and off-label in
526 symptomatic patients[5,55,56]. Such treatments are likely to be most beneficial when
527 applied during early or acute inflammatory disease phases, before irreversible
528 remodeling develops.

529 More targeted approaches, including IL-1β antagonists, have shown promising
530 results in related inflammatory cardiac conditions[57,58]. In *Pkp2*$^{+/-}$ mice, the therapeutic
531 window spans 9-12 months, whereas in patients, the optimal timing remains to be
532 determined and may vary between individuals. Our data align with retrospective
533 clinical studies suggesting that anti-inflammatory therapies could benefit desmoplakin
534 mutation carriers presenting with myocarditis-like symptoms[57,58]. Beyond therapeutic
535 modulation, our findings highlight the influence of secondary triggers on the course of
536 genetic cardiomyopathies. The absence of a cardiac phenotype following MCMV
537 infection in *Ttn*$^{+/-}$ mice suggests that the timing and sequence of second hits are
538 critical for disease manifestation. In humans, *TTN* variants are frequently detected in
539 patients with complicated myocarditis[7], which may reflect a scenario in which pre-
540 existing, subclinical myocardial impairment serves as a first hit that limits recovery
541 after infection and accelerates cardiomyopathy progression. In contrast, the viral
542 challenge in our mouse model, applied before structural changes developed, may
543 have preceded this window of susceptibility. It is conceivable that combining
544 stressors, such as pregnancy, alcohol abuse or toxic substances, with viral infection
545 could unmask such vulnerability in *Ttn*-deficient hearts[10]. In *Pkp2*-deficient hearts,
546 however, latent MCMV proved to be a potent trigger of cardiac dysfunction, a finding
547 with direct translational relevance: patients with PKP2 or other desmosomal

548 mutations may particularly benefit from avoiding physical exertion or promptly
549 treating systemic infections. Preventive measures, including vaccination and early
550 antiviral therapy, should therefore be applied for individuals with a genetic
551 predisposition. Although no CMV vaccine is currently available, antiviral agents such
552 as ganciclovir, routinely used in immunocompromised patients[59], could be explored
553 as adjuncts to anti-inflammatory treatment during early myocarditis-like episodes. In
554 conclusion, our findings emphasize infection control and timely immunomodulation as
555 promising strategies to delay or prevent disease progression in ACM.

556 This study also has limitations that should be considered when interpreting the
557 results. As with any mouse model, the immune and inflammatory responses
558 characterized here may not fully capture the complexity of human ACM, where
559 genetic diversity, lifelong antigen exposure and comorbidities shape disease
560 expression. In addition, only male mice were included in the MCMV-infected *Pkp2*$^{+/-}$
561 cohort, reflecting the known male predominance in ACM, but future work should
562 examine whether sex-specific immune responses modify the disease trajectory. Our
563 findings in *Ttn*$^{+/-}$ mice represent a single truncating variant located in the A-band and
564 therefore do not exclude the possibility that other variants and location in titin and in
565 particular additional environmental triggers could interact with inflammation
566 differently. Finally, while CCR2^{+} monocytes emerged as a shared disease-driving
567 population across desmosomal cardiomyopathy models, their essential role in human
568 host defense limits the direct translational applicability of cell-depletion strategies.

569 Despite these considerations, the convergence of genetic, immunological, and
570 virological evidence across models provides strong support for early inflammatory
571 signaling as a central driver of desmosomal cardiomyopathy and highlights the
572 importance of defining clinically meaningful windows for therapeutic intervention.

7. Acknowledgements

The authors thank Anne Kilinç, Susanne Schraut and Daniela Urlaub for their dedicated technical assistance with mouse scoring, genotyping, and experimental procedures; Arnhild Grothey for providing the viral stocks; and Berkan Arslan for performing and analyzing echocardiographic measurements. Alicia Bender and Jakob Weilbach are acknowledged for their support during tissue collection, Sonja Luckhardt for expert technical assistance with cytokine profiling, and Alanis Barbosa Gulde for conducting the kinase activity analyses. We acknowledge the contributions of service projects PS1 and PS2 within the Collaborative Research Centre 1525 for their support in conducting echocardiography and supporting CITE-seq and single-cell transcriptomic profiling, respectively. Schematic subfigures were created in BioRender; Gerull, B. (2025) https://BioRender.com/hkmxgxg.

8. Sources of Funding

CC, GCR, SF, LD and BG received support from the German Research Foundation as part of the Collaborative Research Centre 1525 'Cardio-Immune Interfaces' (grant number 453989101). BG received funding from the German Heart Foundation (Deutsche Herzstiftung e.V. 'Plötzlicher Herztod'). MN was supported by the Otto Hess research fellowship of the German Cardiac Society (DGK). JK and SK received scholarships of the Graduate School of Life Science (GSLS), Würzburg.

9. Disclosures

None.

10. Supplemental Material

Supplemental Methods

Supplemental Figures

Supplemental Tables

References[11,30,44,60-78]

11. References

1. Schulz-Menger J, Collini V, Groschel J, Adler Y, Brucato A, Christian V, Ferreira VM, Gandjbakhch E, Heidecker B, Kerneis M, et al. 2025 ESC Guidelines for the management of myocarditis and pericarditis. *Eur Heart J*. 2025;46:3952–4041. doi: 10.1093/eurheartj/ehaf192
2. Bassetto G, Angriman F, Gava CPLD, Paldino A, Perotto M, Bordignon L, Gigli M, Ferro MD, Massa L, Altinier A, et al. Hot Phases Cardiomyopathy: Pathophysiology, Diagnostic Challenges, and Emerging Therapies. *Current Cardiology Reports*. 2025;27. doi: 10.1007/s11886-024-02168-6
3. Asatryan B, Asimaki A, Landstrom AP, Khanji MY, Odening KE, Cooper LT, Marchlinski FE, Gelzer AR, Semsarian C, Reichlin T, et al. Inflammation and Immune Response in Arrhythmogenic Cardiomyopathy: State-of-the-Art Review. *Circulation*. 2021;144:1646–1655. doi: 10.1161/CIRCULATIONAHA.121.055890
4. Gerull B, Heuser A, Wichter T, Paul M, Basson CT, McDermott DA, Lerman BB, Markowitz SM, Ellinor PT, MacRae CA, et al. Mutations in the desmosomal protein plakophilin-2 are common in arrhythmogenic right ventricular cardiomyopathy. *Nat Genet*. 2004;36:1162–1164. doi: 10.1038/ng1461
5. Peretto G, Barzaghi F, Cicalese MP, Di Resta C, Slavich M, Benedetti S, Giangiobbe S, Rizzo S, Palmisano A, Esposito A, et al. Immunosuppressive therapy in childhood-onset arrhythmogenic inflammatory cardiomyopathy. *Pacing and Clinical Electrophysiology*. 2021;44:552–556. doi: 10.1111/pace.14153
6. Martins D, Ovaert C, Khraiche D, Boddaert N, Bonnet D, Raimondi F. Myocardial inflammation detected by cardiac MRI in Arrhythmogenic right ventricular cardiomyopathy: A paediatric case series. *Int J Cardiol*. 2018;271:81–86. doi: 10.1016/j.ijcard.2018.05.116
7. Monda E, Bakalakos A, Cannie D, O'Mahony C, Syrris P, Kaski JP, Limongelli G, Elliott PM. Prevalence of Pathogenic Variants in Cardiomyopathy-Associated Genes in Acute Myocarditis: A Systematic Review and Meta-Analysis. *JACC Heart Fail*. 2024;12:1101–1111. doi: 10.1016/j.jchf.2024.02.012
8. Ammirati E, Raimondi F, Piriou N, Sardo Infirri L, Mohiddin SA, Mazzanti A, Shenoy C, Cavallari UA, Imazio M, Aquaro GD, et al. Acute Myocarditis Associated With Desmosomal Gene Variants. *JACC Heart Fail*. 2022;10:714–727. doi: 10.1016/j.jchf.2022.06.013
9. Gerull B, Gramlich M, Atherton J, McNabb M, Trombitas K, Sasse-Klaassen S, Seidman JG, Seidman C, Granzier H, Labeit S, et al. Mutations of TTN, encoding the giant muscle filament titin, cause familial dilated cardiomyopathy. *Nat Genet*. 2002;30:201–204. doi: 10.1038/ng815
10. Verdonschot JAJ, Heymans SRB. Dilated cardiomyopathy: second hits knock-down the heart. *European Heart Journal*. 2024;45:500–501. doi: 10.1093/eurheartj/ehad778
11. Gramlich M, Michely B, Krohne C, Heuser A, Erdmann B, Klaassen S, Hudson B, Magarin M, Kirchner F, Todiras M, et al. Stress-induced dilated cardiomyopathy in a knock-in mouse model mimicking human titin-based disease. *J Mol Cell Cardiol*. 2009;47:352–358. doi: 10.1016/j.yjmcc.2009.04.014
12. Kažukauskienė I, Baltrūnienė V, Jakubauskas A, Žurauskas E, Maneikienė VV, Daunoravičius D, Čelutkienė J, Ručinskas K, Grabauskienė V. Prevalence and prognostic relevance of myocardial inflammation and cardiotropic viruses in non-ischemic dilated cardiomyopathy. *Cardiology Journal*. 2022;29:441–453. doi: 10.5603/cj.a2020.0088
13. Wang H, Peng G, Bai J, He B, Huang K, Hu X, Liu D. Cytomegalovirus Infection and Relative Risk of Cardiovascular Disease (Ischemic Heart Disease, Stroke, and Cardiovascular Death): A Meta-Analysis of Prospective Studies Up to 2016. *J Am Heart Assoc*. 2017;6. doi: 10.1161/JAHA.116.005025

14. Spray L, McIntosh A, McCartney PJ, Macfarlane PW, Maznyczka A, Welsh P, Berry C, Spyridopoulos I. Latent Cytomegalovirus Infection Is Associated With Impaired Left Ventricular Function After ST-Segment–Elevation Myocardial Infarction. *Journal of the American Heart Association*. 2025;14. doi: 10.1161/jaha.124.040584
15. Bonavita CM, Cardin RD. Don't Go Breaking My Heart: MCMV as a Model for HCMV-Associated Cardiovascular Diseases. *Pathogens*. 2021;10:619. doi: 10.3390/pathogens10050619
16. Hoorntje ET, Te Rijdt WP, James CA, Pilichou K, Basso C, Judge DP, Bezzina CR, Van Tintelen JP. Arrhythmogenic cardiomyopathy: pathology, genetics, and concepts in pathogenesis. *Cardiovascular Research*. 2017;113:1521–1531. doi: 10.1093/cvr/cvx150
17. Chelko SP, Asimaki A, Andersen P, Bedja D, Amat-Alarcon N, Demazumder D, Jasti R, Macrae CA, Leber R, Kleber AG, et al. Central role for GSK3β in the pathogenesis of arrhythmogenic cardiomyopathy. *JCI Insight*. 2016;1. doi: 10.1172/jci.insight.85923
18. Ng KE, Delaney PJ, Thenet D, Murtough S, Webb CM, Zaman N, Tsisanova E, Mastroianni G, Walker SLM, Westaby JD, et al. Early inflammation precedes cardiac fibrosis and heart failure in desmoglein 2 murine model of arrhythmogenic cardiomyopathy. *Cell and Tissue Research*. 2021;386:79–98. doi: 10.1007/s00441-021-03488-7
19. Van Opbergen CJM, Noorman M, Pfenniger A, Copier JS, Vermij SH, Li Z, Van Der Nagel R, Zhang M, De Bakker JMT, Glass AM, et al. Plakophilin-2 Haploinsufficiency Causes Calcium Handling Deficits and Modulates the Cardiac Response Towards Stress. *International Journal of Molecular Sciences*. 2019;20:4076. doi: 10.3390/ijms20174076
20. Bubić I, Wagner M, Krmpotić A, Saulig T, Kim S, Yokoyama WM, Jonjić S, Koszinowski UH. Gain of Virulence Caused by Loss of a Gene in Murine Cytomegalovirus. *Journal of Virology*. 2004;78:7536–7544. doi: 10.1128/jvi.78.14.7536-7544.2004
21. Li Y, Xiao J, Li C, Yang M. Memory inflation: Beyond the acute phase of viral infection. *Cell Proliferation*. 2024;57. doi: 10.1111/cpr.13705
22. Yang S, Penna V, Lavine KJ. Functional diversity of cardiac macrophages in health and disease. *Nature Reviews Cardiology*. 2025;22:431–442. doi: 10.1038/s41569-024-01109-8
23. Deshmane SL, Kremlev S, Amini S, Sawaya BE. Monocyte chemoattractant protein-1 (MCP-1): an overview. *J Interferon Cytokine Res*. 2009;29:313–326. doi: 10.1089/jir.2008.0027
24. Huang L. The role of IL-17 family cytokines in cardiac fibrosis. *Frontiers in Cardiovascular Medicine*. 2024;11. doi: 10.3389/fcvm.2024.1470362
25. Lasrado N, Reddy J. An overview of the immune mechanisms of viral myocarditis. *Reviews in Medical Virology*. 2020;30:1–14. doi: 10.1002/rmv.2131
26. Alam F, Singh A, Flores-Malavet V, Sell S, Cooper AM, Swain SL, McKinstry KK, Strutt TM. CD25-Targeted IL-2 Signals Promote Improved Outcomes of Influenza Infection and Boost Memory CD4 T Cell Formation. *The Journal of Immunology*. 2020;204:3307–3314. doi: 10.4049/jimmunol.2000205
27. Ruan C-C, Kong L-R, Chen X-H, Ma Y, Pan X-X, Zhang Z-B, Gao P-J. A2A Receptor Activation Attenuates Hypertensive Cardiac Remodeling via Promoting Brown Adipose Tissue-Derived FGF21. *Cell Metabolism*. 2018;28:476–489.e475. doi: 10.1016/j.cmet.2018.06.013
28. Planavila A, Redondo-Angulo I, Ribas F, Garrabou G, Casademont J, Giralt M, Villarroya F. Fibroblast growth factor 21 protects the heart from oxidative stress. *Cardiovascular Research*. 2015;106:19–31. doi: 10.1093/cvr/cvu263
29. Gramlich M, Pane LS, Zhou Q, Chen Z, Murgia M, Schötterl S, Goedel A, Metzger K, Brade T, Parrotta E, et al. Antisense-mediated exon skipping: a therapeutic strategy for titin-based dilated cardiomyopathy. *EMBO Molecular Medicine*. 2015;7:562–576. doi: 10.15252/emmm.201505047

30. Dann E, Henderson NC, Teichmann SA, Morgan MD, Marioni JC. Differential abundance testing on single-cell data using k-nearest neighbor graphs. *Nat Biotechnol*. 2022;40:245–253. doi: 10.1038/s41587-021-01033-z
31. Ferrucci L, Fabbri E. Inflammageing: chronic inflammation in ageing, cardiovascular disease, and frailty. *Nature Reviews Cardiology*. 2018;15:505–522. doi: 10.1038/s41569-018-0064-2
32. Gong Q, Sharma M, Glass MC, Kuan EL, Chander A, Singh M, Graybuck LT, Thomson ZJ, LaFrance CM, Rachid Zaim S, et al. Multi-omic profiling reveals age-related immune dynamics in healthy adults. *Nature*. 2025. doi: 10.1038/s41586-025-09686-5
33. Zhang J, Tian M, Xia Z, Feng P. Roles of IκB kinase ε in the innate immune defense and beyond. *Virologica Sinica*. 2016;31:457–465. doi: 10.1007/s12250-016-3898-y
34. Storz P. Protein kinase D mediates a stress-induced NF-kappaB activation and survival pathway. *The EMBO Journal*. 2003;22:109–120. doi: 10.1093/emboj/cdg009
35. Ersahin T, Tuncbag N, Cetin-Atalay R. The PI3K/AKT/mTOR interactive pathway. *Molecular BioSystems*. 2015;11:1946–1954. doi: 10.1039/c5mb00101c
36. Brühl H, Cihak J, Plachý J, Kunz-Schughart L, Niedermeier M, Denzel A, Rodriguez Gomez M, Talke Y, Luckow B, Stangassinger M, et al. Targeting of Gr-1+,CCR2+ monocytes in collagen-induced arthritis. *Arthritis & Rheumatism*. 2007;56:2975–2985. doi: 10.1002/art.22854
37. Fowler K, Mucha J, Neumann M, Lewandowski W, Kaczanowska M, Grys M, Schmidt E, Natenshon A, Talarico C, Buck PO, et al. A systematic literature review of the global seroprevalence of cytomegalovirus: possible implications for treatment, screening, and vaccine development. *BMC Public Health*. 2022;22. doi: 10.1186/s12889-022-13971-7
38. Heald-Sargent TA, Forte E, Liu X, Thorp EB, Abecassis MM, Zhang ZJ, Hummel MA. New Insights Into the Molecular Mechanisms and Immune Control of Cytomegalovirus Reactivation. *Transplantation*. 2020;104:e118–e124. doi: 10.1097/TP.0000000000003138
39. Mitrović M, Arapović J, Jordan S, Fodil-Cornu N, Ebert S, Vidal SM, Krmpotić A, Reddehase MJ, Jonjić S. The NK Cell Response to Mouse Cytomegalovirus Infection Affects the Level and Kinetics of the Early CD8⁺T-Cell Response. *Journal of Virology*. 2012;86:2165–2175. doi: 10.1128/jvi.06042-11
40. Griessl M, Renzaho A, Freitag K, Seckert CK, Reddehase MJ, Lemmermann NAW. Stochastic Episodes of Latent Cytomegalovirus Transcription Drive CD8 T-Cell “Memory Inflation” and Avoid Immune Evasion. *Frontiers in Immunology*. 2021;12. doi: 10.3389/fimmu.2021.668885
41. Chen X, Peng Y, Ge S, Li Y. Inflammation and cardiac dysfunction during sepsis, muscular dystrophy, and myocarditis. *Burns & Trauma*. 2013;1:109. doi: 10.4103/2321-3868.123072
42. Asimaki A, Tandri H, Duffy ER, Winterfield JR, Mackey-Bojack S, Picken MM, Cooper LT, Wilber DJ, Marcus FI, Basso C, et al. Altered Desmosomal Proteins in Granulomatous Myocarditis and Potential Pathogenic Links to Arrhythmogenic Right Ventricular Cardiomyopathy. *Circulation: Arrhythmia and Electrophysiology*. 2011;4:743–752. doi: 10.1161/circep.111.964890
43. Lubos N, Van Der Gaag S, Gerçek M, Kant S, Leube RE, Krusche CA. Inflammation shapes pathogenesis of murine arrhythmogenic cardiomyopathy. *Basic Research in Cardiology*. 2020;115. doi: 10.1007/s00395-020-0803-5
44. Rizzo G, Gropper J, Piollet M, Vafadarnejad E, Rizakou A, Bandi SR, Arampatzi P, Krammer T, DiFabion N, Dietrich O, et al. Dynamics of monocyte-derived macrophage diversity in experimental myocardial infarction. *Cardiovasc Res*. 2023;119:772–785. doi: 10.1093/cvr/cvac113
45. Duan X, Zhang L, Liu K, Guo K, You Y, Jia H, Zhou S, Han B. Macrophage-derived SPP1 exacerbate myocardial injury by interacting with fibroblasts in viral myocarditis. *Biology Direct*. 2025;20. doi: 10.1186/s13062-025-00621-2

46. Feng G, Bajpai G, Ma P, Koenig A, Bredemeyer A, Lokshina I, Lai L, Forster I, Leuschner F, Kreisel D, et al. CCL17 Aggravates Myocardial Injury by Suppressing Recruitment of Regulatory T Cells. *Circulation*. 2022;145:765–782. doi: 10.1161/CIRCULATIONAHA.121.055888
47. Yousif LI, Tanja AA, De Boer RA, Teske AJ, Meijers WC. The role of immune checkpoints in cardiovascular disease. *Frontiers in Pharmacology*. 2022;13. doi: 10.3389/fphar.2022.989431
48. Deleon-Pennell KY, Iyer RP, Ero OK, Cates CA, Flynn ER, Cannon PL, Jung M, Shannon DA, Garrett MR, Buchanan W, et al. Periodontal-induced chronic inflammation triggers macrophage secretion of Ccl12 to inhibit fibroblast-mediated cardiac wound healing. *JCI Insight*. 2017;2. doi: 10.1172/jci.insight.94207
49. Baruzzi A, Iacobucci I, Soverini S, Lowell CA, Martinelli G, Berton G. c-Abl and Src-family kinases cross-talk in regulation of myeloid cell migration. *FEBS Lett*. 2010;584:15–21. doi: 10.1016/j.febslet.2009.11.009
50. Liang Y, Ye L. Bound to be perfect: Lck and T cell co-receptors. *Nature Immunology*. 2023;24:5–7. doi: 10.1038/s41590-022-01392-y
51. Parsons SA, Greer PA. The Fps/Fes kinase regulates the inflammatory response to endotoxin through down-regulation of TLR4, NF-κB activation, and TNF-α secretion in macrophages. *Journal of Leukocyte Biology*. 2006;80:1522–1528. doi: 10.1189/jlb.0506350
52. Chelko SP, Penna VR, Engel M, Shiel EA, Centner AM, Farra W, Cannon EN, Landim-Vieira M, Schaible N, Lavine K, et al. NFκB signaling drives myocardial injury via CCR2+ macrophages in a preclinical model of arrhythmogenic cardiomyopathy. *Journal of Clinical Investigation*. 2024;134. doi: 10.1172/jci172014
53. Pérez-Hernández M, Marrón-Liñares GM, Schlamp F, Heguy A, Van Opbergen CJM, Mezzano V, Zhang M, Liang F-X, Cerrone M, Delmar M. Transcriptomic Coupling of PKP2 With Inflammatory and Immune Pathways Endogenous to Adult Cardiac Myocytes. *Frontiers in Physiology*. 2021;11. doi: 10.3389/fphys.2020.623190
54. Nahrendorf M, Pittet MJ, Swirski FK. Monocytes: protagonists of infarct inflammation and repair after myocardial infarction. *Circulation*. 2010;121:2437–2445. doi: 10.1161/CIRCULATIONAHA.109.916346
55. Chimenti C, Russo MA, Frustaci A. Immunosuppressive therapy in virus-negative inflammatory cardiomyopathy: 20-year follow-up of the TIMIC trial. *Eur Heart J*. 2022;43:3463–3473. doi: 10.1093/eurheartj/ehac348
56. Gasperetti A, Muller SA, Peretto G, Asatryan B, Protonotarios A, Laredo M, Tarlet P-Y, Syrris P, Carrick RT, Murray B, et al. Prognostic Role of Myocarditis-Like Episodes and Their Treatment in Patients With Pathogenic Desmoplakin Variants. *Circulation*. 2025. doi: 10.1161/circulationaha.125.073919
57. Gasperetti A, Carrick RT, Muller S, Murray B, Adamo L, Bauce B, McNally E, Helms A. Desmoplakin Cardiomyopathy: Role of Inflammation and Potential Role of Disease-Modifying Therapies. *Current Cardiology Reports*. 2025;27. doi: 10.1007/s11886-024-02183-7
58. Lopez RI, Marchetta M, Ayers M, Mason P, Thomas M, Gasperetti A, Gilotra NA, Abbate A. Desmoplakin Cardiomyopathy Presenting With Recurrent Myopericarditis Responsive to Interleukin-1 Blockade. *JACC Case Rep*. 2025;30:104039. doi: 10.1016/j.jaccas.2025.104039
59. Kotton CN, Kamar N. New Insights on CMV Management in Solid Organ Transplant Patients: Prevention, Treatment, and Management of Resistant/Refractory Disease. *Infectious Diseases and Therapy*. 2023;12:333–342. doi: 10.1007/s40121-022-00746-1
60. Zinke R. A functional characterization of Plakophilin-2 and Desmoplakin in the adult mouse heart. . In; A functional characterization of Plakophilin–2 and Desmoplakin in the adult mouse heart. Doctoral thesis, FU Berlin, Berlin, Germany. 2013; Retrieved from https://refubium.fu–berlin.de/handle/fub188/13779.

61. Puhl SL, Weeks KL, Ranieri A, Avkiran M. Assessing structural and functional responses of murine hearts to acute and sustained beta-adrenergic stimulation in vivo. *J Pharmacol Toxicol Methods*. 2016;79:60–71. doi: 10.1016/j.vascn.2016.01.007
62. Sacher T, Podlech J, Mohr CA, Jordan S, Ruzsics Z, Reddehase MJ, Koszinowski UH. The major virus-producing cell type during murine cytomegalovirus infection, the hepatocyte, is not the source of virus dissemination in the host. *Cell Host Microbe*. 2008;3:263–272. doi: 10.1016/j.chom.2008.02.014
63. Tischer BK, Smith GA, Osterrieder N. En passant mutagenesis: a two step markerless red recombination system. *Methods Mol Biol*. 2010;634:421–430. doi: 10.1007/978-1-60761-652-8_30
64. Brune W, Hengel H, Koszinowski UH. A mouse model for cytomegalovirus infection. *Curr Protoc Immunol*. 2001;Chapter 19:Unit 19 17. doi: 10.1002/0471142735.im1907s43
65. Mack M, Cihak J, Simonis C, Luckow B, Proudfoot AE, Plachy J, Bruhl H, Frink M, Anders HJ, Vielhauer V, et al. Expression and characterization of the chemokine receptors CCR2 and CCR5 in mice. *J Immunol*. 2001;166:4697–4704. doi: 10.4049/jimmunol.166.7.4697
66. Cardiff RD, Miller CH, Munn RJ. Manual hematoxylin and eosin staining of mouse tissue sections. *Cold Spring Harb Protoc*. 2014;2014:655–658. doi: 10.1101/pdb.prot073411
67. Rueden CT, Schindelin J, Hiner MC, DeZonia BE, Walter AE, Arena ET, Eliceiri KW. ImageJ2: ImageJ for the next generation of scientific image data. *BMC Bioinformatics*. 2017;18:529. doi: 10.1186/s12859-017-1934-z
68. Kammerer J, Cirnu A, Williams T, Hasselmeier M, Norpel M, Chen R, Gerull B. Macro-based collagen quantification and segmentation in picrosirius red-stained heart sections using light microscopy. *Biol Methods Protoc*. 2024;9:bpae027. doi: 10.1093/biomethods/bpae027
69. Zillikens H, Kasprick A, Osterloh C, Gross N, Radziewitz M, Hass C, Hartmann V, Behnen-Harer M, Ernst N, Boch K, et al. Topical Application of the PI3Kbeta-Selective Small Molecule Inhibitor TGX-221 Is an Effective Treatment Option for Experimental Epidermolysis Bullosa Acquisita. *Front Med (Lausanne)*. 2021;8:713312. doi: 10.3389/fmed.2021.713312
70. Szklarczyk D, Nastou K, Koutrouli M, Kirsch R, Mehryary F, Hachilif R, Hu D, Peluso ME, Huang Q, Fang T, et al. The STRING database in 2025: protein networks with directionality of regulation. *Nucleic Acids Res*. 2025;53:D730–D737. doi: 10.1093/nar/gkae1113
71. Metz KS, Deoudes EM, Berginski ME, Jimenez-Ruiz I, Aksoy BA, Hammerbacher J, Gomez SM, Phanstiel DH. Coral: Clear and Customizable Visualization of Human Kinome Data. *Cell Syst*. 2018;7:347–350 e341. doi: 10.1016/j.cels.2018.07.001
72. Team RC. R: A Language and Environment for Statistical Computing. https://www.R-project.org/. 2023.
73. Stoeckius M, Hafemeister C, Stephenson W, Houck-Loomis B, Chattopadhyay PK, Swerdlow H, Satija R, Smibert P. Simultaneous epitope and transcriptome measurement in single cells. *Nat Methods*. 2017;14:865–868. doi: 10.1038/nmeth.4380
74. Stoeckius M, Zheng S, Houck-Loomis B, Hao S, Yeung BZ, Mauck WM, 3rd, Smibert P, Satija R. Cell Hashing with barcoded antibodies enables multiplexing and doublet detection for single cell genomics. *Genome Biol*. 2018;19:224. doi: 10.1186/s13059-018-1603-1
75. Stuart T, Butler A, Hoffman P, Hafemeister C, Papalexi E, Mauck WM, 3rd, Hao Y, Stoeckius M, Smibert P, Satija R. Comprehensive Integration of Single-Cell Data. *Cell*. 2019;177:1888–1902 e1821. doi: 10.1016/j.cell.2019.05.031
76. McGinnis CS, Murrow LM, Gartner ZJ. DoubletFinder: Doublet Detection in Single-Cell RNA Sequencing Data Using Artificial Nearest Neighbors. *Cell Syst*. 2019;8:329–337 e324. doi: 10.1016/j.cels.2019.03.003

77. Korsunsky I, Millard N, Fan J, Slowikowski K, Zhang F, Wei K, Baglaenko Y, Brenner M, Loh PR, Raychaudhuri S. Fast, sensitive and accurate integration of single-cell data with Harmony. *Nat Methods*. 2019;16:1289–1296. doi: 10.1038/s41592-019-0619-0

78. Kuleshov MV, Jones MR, Rouillard AD, Fernandez NF, Duan Q, Wang Z, Koplev S, Jenkins SL, Jagodnik KM, Lachmann A, et al. Enrichr: a comprehensive gene set enrichment analysis web server 2016 update. *Nucleic Acids Res*. 2016;44:W90–97. doi: 10.1093/nar/gkw377

881 **12. Figures and Figure Legends**

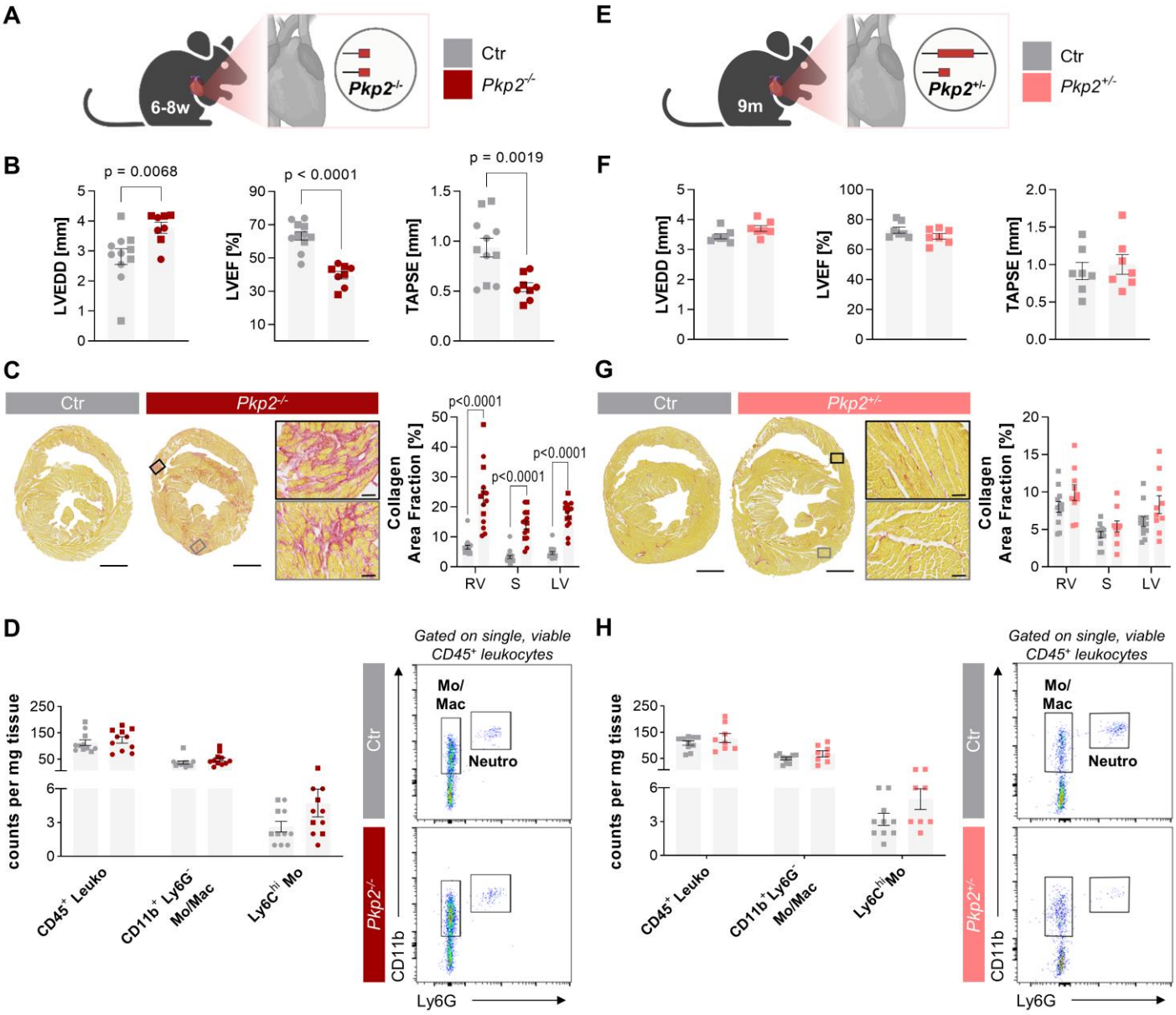

Figure 1. Heterozygous *Pkp2* deficiency does not impact cardiac structure and function, while homozygous loss of *Pkp2* leads to early cardiomyopathy.

A, Scheme of homozygous cardiac-specific *Pkp2* knockout (*Pkp2*$^{-/-}$) mouse model; signature colors: Ctr – grey, *Pkp2*$^{-/-}$ dark red. **B**, Quantification of echocardiographic parameters at 6-8 weeks; Ctr n = 11, *Pkp2*$^{-/-}$ n = 8. **C**, Picrosirius red (PSR) stained cardiac cross-sections and quantification of collagen area fraction; scale bars: overview 1000µm, detail 50µm; Ctr n = 17, *Pkp2*$^{-/-}$ n = 14. **D**, Quantification of different cardiac CD45^{+} leukocytes by flow cytometry in counts per milligram tissue; representative dot plots showing monocytes/macrophages and neutrophils; Ctr n = 11, *Pkp2*$^{-/-}$ n = 11. **E**, Scheme of heterozygous cardiac-specific *Pkp2* knockout (*Pkp2*$^{+/-}$) mouse model; signature colors: Ctr – grey, *Pkp2*$^{+/-}$ pink. **F**, Quantification of echocardiographic parameters at 9 months; Ctr n = 7, *Pkp2*$^{+/-}$ n = 7. **G**, PSR stained cardiac cross-sections and quantification of collagen area fraction; scale bars: overview 1000µm, detail 50µm; Ctr n = 12, *Pkp2*$^{+/-}$ n = 10. **H**, Quantification of different cardiac CD45^{+} leukocytes by flow cytometry in counts per milligram tissue; representative gating showing monocytes/macrophages and neutrophils; Ctr n = 10, *Pkp2*$^{+/-}$ n = 8. Data as mean ± SEM. Male: squares; female: circles. Unpaired t test (± Welch's correction) or Mann–Whitney test, as appropriate. Ctr – control, LVEDD – left ventricular end-diastolic diameter, LVEF – left ventricular ejection fraction, TAPSE – tricuspid annular plane systolic excursion, RV – right ventricle, S – septum, LV – left ventricle, Leuko – leukocytes, Mo/Mac – monocytes/macrophages, Mo – monocytes, Neutro – neutrophils.

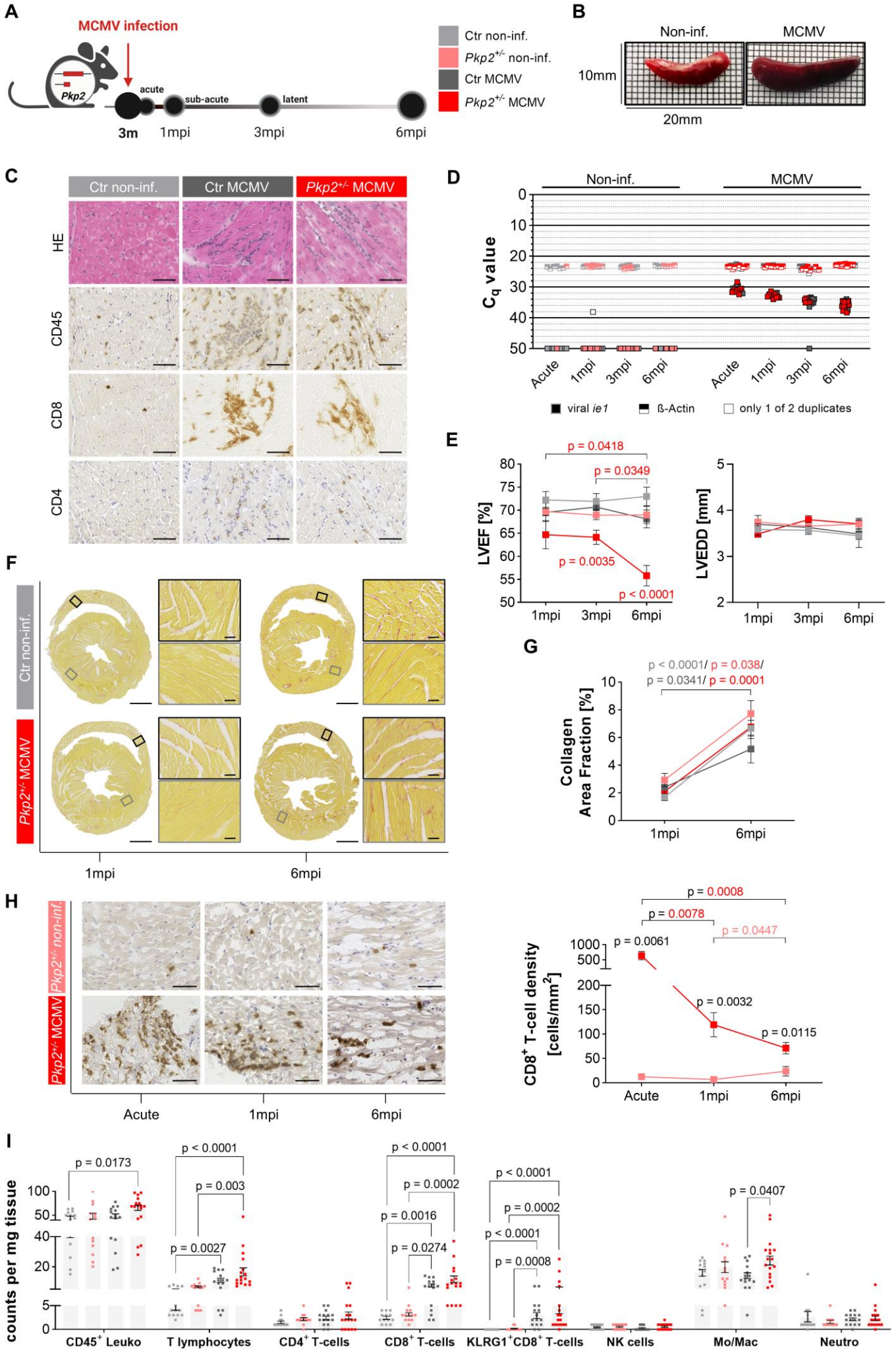
A
MCMV infection
Pkp2
acute
sub-acute
latent
3m
1mpi
3mpi
6mpi
Ctr non-inf.
Pkp2+/- non-inf.
Ctr MCMV
Pkp2+/- MCMV
B
Non-inf.
MCMV
10mm
20mm
C
Ctr non-inf.
Ctr MCMV
Pkp2+/- MCMV
HE
CD45
CD8
CD4
D
Non-inf.
MCMV
Cq value
Acute
1mpi
3mpi
6mpi
viral ie1
ß-Actin
only 1 of 2 duplicates
E
p = 0.0418
p = 0.0349
p = 0.0035
p < 0.0001
LVEF [%]
LVEDD [mm]
1mpi
3mpi
6mpi
F
Ctr non-inf.
Pkp2+/- MCMV
1mpi
6mpi
G
p < 0.0001/ p = 0.038/
p = 0.0341/ p = 0.0001
Collagen Area Fraction [%]
1mpi
6mpi
H
Pkp2+/- non-inf.
Pkp2+/- MCMV
Acute
1mpi
6mpi
p = 0.0008
p = 0.0078
p = 0.0447
p = 0.0061
p = 0.0032
p = 0.0115
CD8+ T-cell density [cells/mm2]
Acute
1mpi
6mpi
I
p = 0.0173
p < 0.0001
p = 0.003
p = 0.0027
p < 0.0001
p = 0.0002
p = 0.0016
p = 0.0274
p < 0.0001
p = 0.0002
p < 0.0001
p = 0.0008
p = 0.0407
counts per mg tissue
CD45+ Leuko
T lymphocytes
CD4+ T-cells
CD8+ T-cells
KLRG1+CD8+ T-cells
NK cells
Mo/Mac
Neutro

Figure 2. MCMV infection accelerates functional cardiac abnormalities in genetically predisposed *Pkp2*$^{+/-}$ mice.

A, Schematic experimental design. 3-month-old *Pkp2*$^{+/-}$ and control (Ctr) mice were infected with 5x10^5 plaque-forming units ∆m157-MCMV-eGFP (MCMV) or received phosphate-buffered saline (PBS) and were analyzed at different time points post-infection. Signature colors: Ctr non-infected (light grey), *Pkp2*$^{+/-}$ non-infected (light pink), Ctr MCMV (dark grey) and *Pkp2*$^{+/-}$ MCMV (red). **B**, Splenomegaly was observed in response to acute MCMV infection. **C**, Representative images of cardiac sections stained with hematoxylin-eosin (HE) and antibodies against the surface markers CD45, CD4 and CD8 during acute infection; scale bar 50µm. **D**, Viral *ie1* (*immediate early 1*, filled squares) and murine ß-actin (half-top-filled squares) DNA copies detected by quantitative polymerase-chain reaction in heart samples from acute to latent infection represented by quantification cycle values (C_q). Measurements were performed in technical duplicates. It is indicated by an unfilled symbol when only one value was usable; n = Acute/1mpi/3mpi/6mpi: Ctr non-infected n = 6/6/6/4, *Pkp2*$^{+/-}$ non-infected n = 1/7/8/4, Ctr MCMV n = 6/6/9/8, *Pkp2*$^{+/-}$ MCMV n = 8/9/6/13. **E**, Quantification of echocardiographic parameters from 1 to 6 months post-infection (mpi); n = 1mpi/3mpi/6mpi: Ctr non-infected n = 6/9/7, *Pkp2*$^{+/-}$ non-infected n = 7/10/7, Ctr MCMV n = 6/14/5, *Pkp2*$^{+/-}$ MCMV n = 8/13/7. **F+G**, Representative picrosirius red staining of cardiac sections and quantification of collagen area fraction at 1 and 6mpi; scale bars: overview 1000µm, detail 50µm; n = 1mpi/6mpi: Ctr non-infected n = 4/12, *Pkp2*$^{+/-}$ non-infected n = 5/9, Ctr MCMV n = 2/10, *Pkp2*$^{+/-}$ MCMV n = 9/12. **H**, Representative images of CD8$^+$ immunostaining and quantification of CD8$^+$ T-cell density from acute to latent infection; scale bar 50µm; n = Acute/1mpi/3mpi/6mpi: *Pkp2*$^{+/-}$ non-infected n = 4/6/11/9, *Pkp2*$^{+/-}$ MCMV n = 7/11/6/7. **I**, Flow cytometry quantification of cardiac CD45$^+$ leukocytes in absolute counts per milligram tissue at 6mpi; Ctr non-infected n = 13, *Pkp2*$^{+/-}$ non-infected n = 13, Ctr MCMV n = 15, *Pkp2*$^{+/-}$ MCMV n = 17. Data are shown as mean ± SEM. Only male mice were used (square symbol). Ordinary one-way ANOVA with or without Brown-Forsythe and Welch's correction and Tukey's or Dunnett's T3 multiple comparisons, respectively or Kruskal-Wallis test with Dunn's multiple comparisons, as appropriate for >2 groups. Unpaired t test with or without Welch's correction or Mann-Whitney test, as appropriate for 2 groups. P-values in **E** are shown for one group over time (bracket) and across groups at one time point compared to Ctr non-infected. All other p-values can be found in Table S3-S6. m – months, LVEF – left ventricular ejection fraction, LVEDD left ventricular end-diastolic diameter, NK cells – natural killer cells, Mo/Mac – monocytes/macrophages.

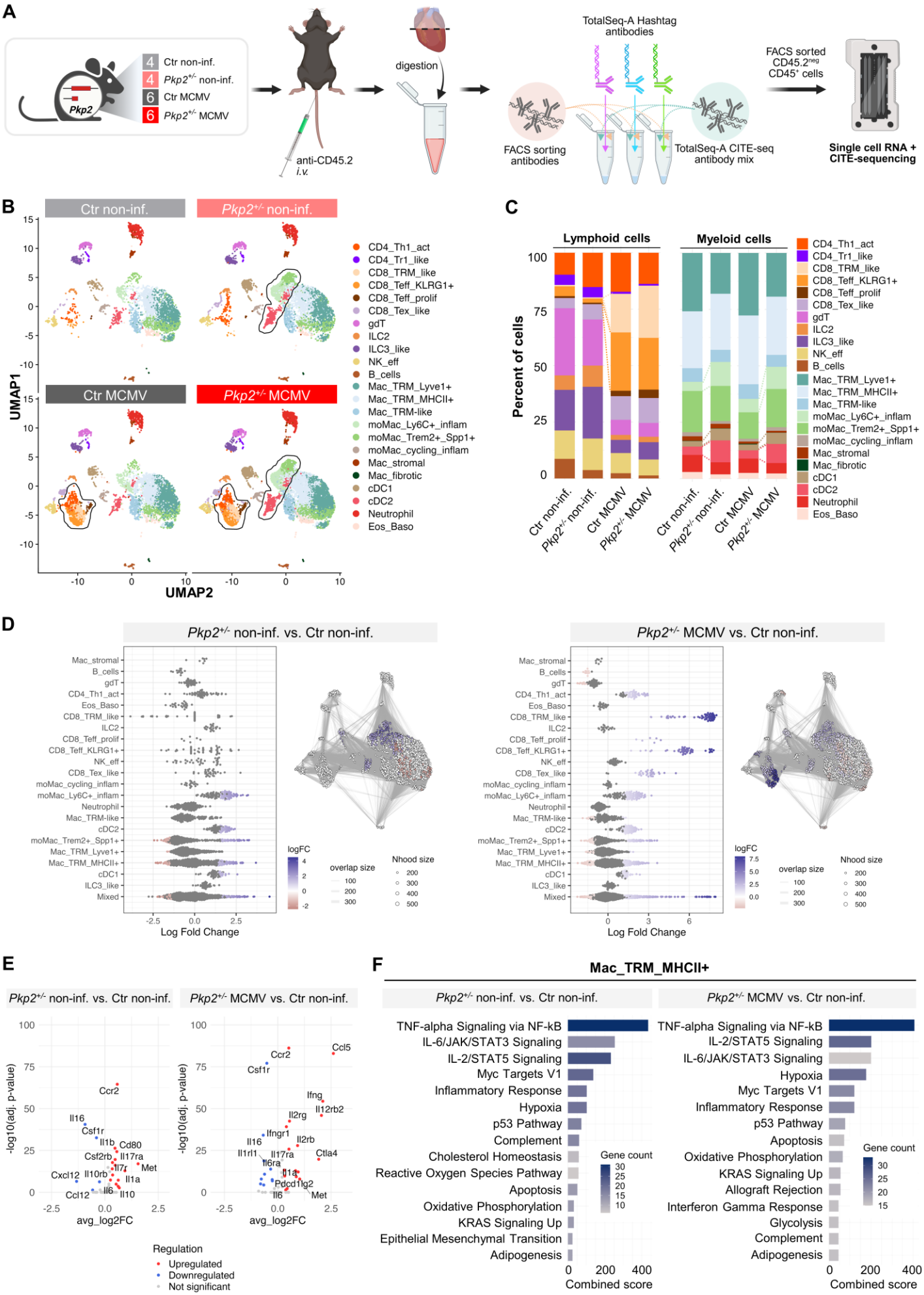
A
Pkp2
4 Ctr non-inf.
4 Pkp2+/- non-inf.
6 Ctr MCMV
6 Pkp2+/- MCMV
anti-CD45.2
i.v.
digestion
TotalSeq-A Hashtag antibodies
FACS sorting antibodies
TotalSeq-A CITE-seq antibody mix
FACS sorted CD45.2neg CD45+ cells
Single cell RNA + CITE-sequencing
B
Ctr non-inf.
Pkp2+/- non-inf.
Ctr MCMV
Pkp2+/- MCMV
UMAP1
UMAP2
CD4_Th1_act
CD4_Tr1_like
CD8_TRM_like
CD8_Teff_KLRG1+
CD8_Teff_prolif
CD8_Tex_like
gdT
ILC2
ILC3_like
NK_eff
B_cells
Mac_TRM_Lyve1+
Mac_TRM_MHCII+
Mac_TRM-like
moMac_Ly6C+_inflam
moMac_Trem2+_Spp1+
moMac_cycling_inflam
Mac_stromal
Mac_fibrotic
cDC1
cDC2
Neutrophil
Eos_Baso
C
Lymphoid cells
Myeloid cells
Percent of cells
Ctr non-inf.
Pkp2+/- non-inf.
Ctr MCMV
Pkp2+/- MCMV
D
Pkp2+/- non-inf. vs. Ctr non-inf.
Pkp2+/- MCMV vs. Ctr non-inf.
Log Fold Change
logFC
overlap size
Nhood size
E
Pkp2+/- non-inf. vs. Ctr non-inf.
Pkp2+/- MCMV vs. Ctr non-inf.
-log10(adj. p-value)
avg_log2FC
Ccr2
Il16
Csf1r
Il1b
Cd80
Csf2rb
Il17ra
Il7r
Met
Cxcl12
Il10rb
Il1a
Ccl12
Il6
Il10
Ccl5
Ifng
Il12rb2
Il2rg
Ifngr1
Il2rb
Il1r1
Il17ra
Ctla4
Il6ra
Il1a
Pdcd1lg2
Regulation
Upregulated
Downregulated
Not significant
F
Mac_TRM_MHCII+
Pkp2+/- non-inf. vs. Ctr non-inf.
Pkp2+/- MCMV vs. Ctr non-inf.
TNF-alpha Signaling via NF-kB
IL-6/JAK/STAT3 Signaling
IL-2/STAT5 Signaling
Myc Targets V1
Inflammatory Response
Hypoxia
p53 Pathway
Complement
Cholesterol Homeostasis
Reactive Oxygen Species Pathway
Apoptosis
Oxidative Phosphorylation
KRAS Signaling Up
Epithelial Mesenchymal Transition
Adipogenesis
Gene count
Combined score

Figure 3. *Pkp2*$^{+/-}$ genotype is sufficient to induce subclinical accumulation of myeloid cell types before cardiac dysfunction emerges.

A, Schematic workflow of the CITE-seq experiment. At 6 months post-infection (mpi), mice received an intravenous (*i.v.*) injection of anti-CD45.2-APC before heart dissociation (ventricles only). Samples were multiplexed with TotalSeq-A hashtags and labeled with CITE-seq antibodies plus CD45 FACS antibody. Circulating cells were excluded by sorting CD45^{+} CD45.2-APC^{-} leukocytes. Two libraries from 10 pooled samples each were sequenced; Ctr non-infected n = 4, *Pkp2*$^{+/-}$ non-infected n = 4, Ctr MCMV n = 6, *Pkp2*$^{+/-}$ MCMV n = 6. **B**, UMAP representation of Seurat clustered leukocytes (in total 26,656) split by experimental group. **C**, Relative abundance of lymphoid and myeloid immune populations across groups. **D**, Assessment of statistically relevant changes in abundance using the MiloR package in *Pkp2*$^{+/-}$ non-infected and *Pkp2*$^{+/-}$ MCMV versus Ctr non-infected, respectively. **E**, Comparative cytokine expression analysis in cardiac leukocytes in *Pkp2*$^{+/-}$ non-infected and *Pkp2*$^{+/-}$ MCMV versus Ctr non-infected, respectively. **F**, Pathway enrichment analysis using MSig_DB_Hallmark_2020 database via the enrichR pipeline on pseudobulk-dataset. Shown are the top upregulated pathways by combined score in the subcluster Mac_TRM_MHCII+ of *Pkp2*$^{+/-}$ non-infected and *Pkp2*$^{+/-}$ MCMV versus Ctr non-infected, respectively. Ctr - control, CITE-seq - cellular indexing of transcriptomes and epitopes by sequencing, FACS – fluorescence-activated cell sorting, UMAP - uniform manifold approximation and projection.

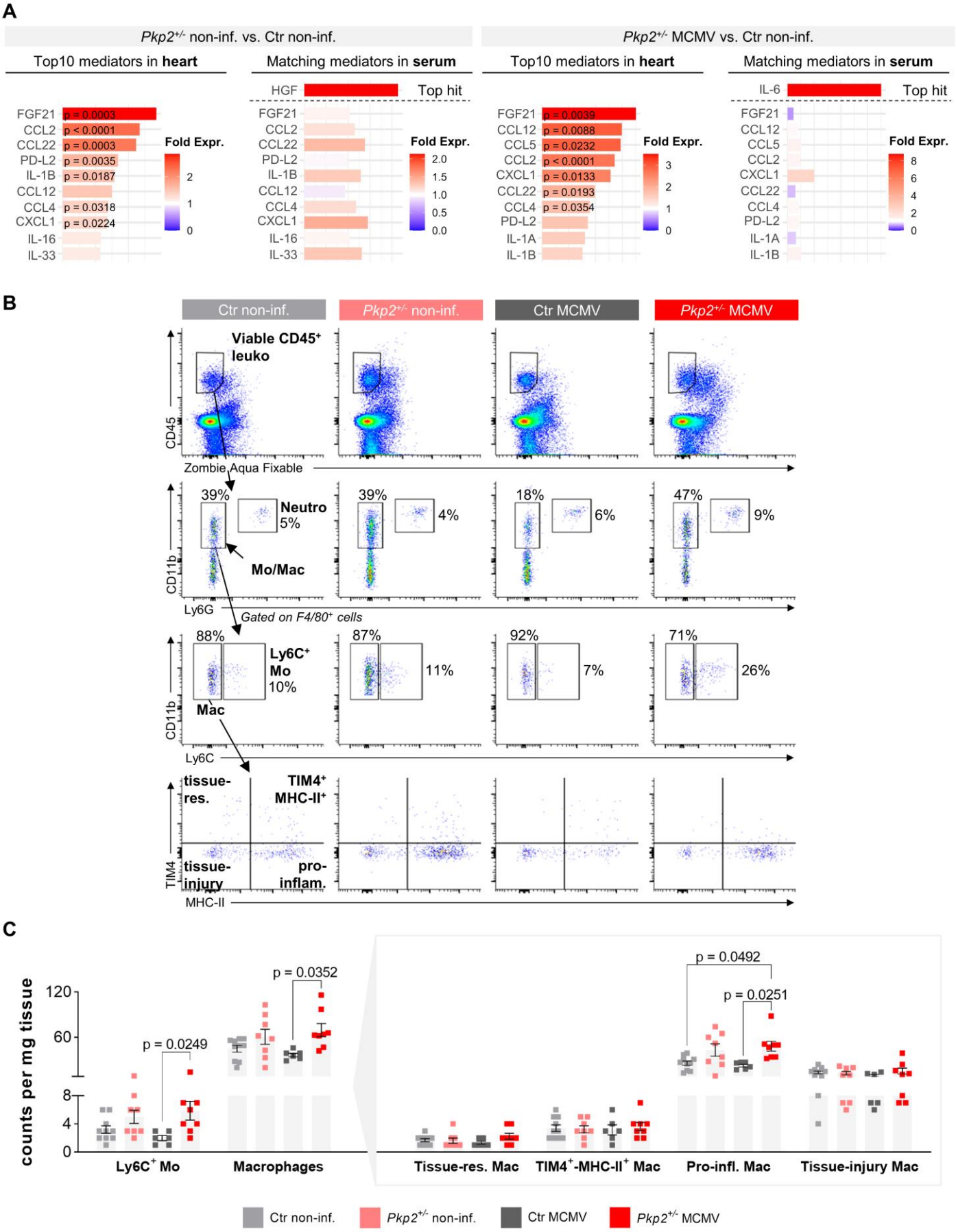
A
Pkp2+/- non-inf. vs. Ctr non-inf.
Top10 mediators in heart
Matching mediators in serum
Pkp2+/- MCMV vs. Ctr non-inf.
Top10 mediators in heart
Matching mediators in serum
FGF21 p = 0.0003
CCL2 p < 0.0001
CCL22 p = 0.0003
PD-L2 p = 0.0035
IL-1B p = 0.0187
CCL12
CCL4 p = 0.0318
CXCL1 p = 0.0224
IL-16
IL-33
HGF Top hit
FGF21 p = 0.0039
CCL12 p = 0.0088
CCL5 p = 0.0232
CCL2 p < 0.0001
CXCL1 p = 0.0133
CCL22 p = 0.0193
CCL4 p = 0.0354
PD-L2
IL-1A
IL-1B
IL-6 Top hit
Fold Expr.
B
Ctr non-inf.
Pkp2+/- non-inf.
Ctr MCMV
Pkp2+/- MCMV
Viable CD45+ leuko
CD45
Zombie Aqua Fixable
39%
Neutro 5%
Mo/Mac
39%
4%
18%
6%
47%
9%
CD11b
Ly6G
Gated on F4/80+ cells
88%
Ly6C+ Mo 10%
Mac
87%
11%
92%
7%
71%
26%
Ly6C
tissue-res.
TIM4+ MHC-II+
tissue-injury
pro-inflam.
TIM4
MHC-II
C
counts per mg tissue
120
60
8
4
0
p = 0.0249
p = 0.0352
p = 0.0492
p = 0.0251
Ly6C+ Mo
Macrophages
Tissue-res. Mac
TIM4+-MHC-II+ Mac
Pro-infl. Mac
Tissue-injury Mac
Ctr non-inf.
Pkp2+/- non-inf.
Ctr MCMV
Pkp2+/- MCMV

965 **Figure 4. Heart-specific subclinical upregulation of cytokines in non-infected**
966 ***Pkp2*$^{+/-}$ mice.**

967 **A**, Cytokine profiling based on proximity extension assay at 6 months post-infection
968 (mpi). Shown are the top 10 differentially expressed heart mediators with
969 corresponding serum levels, plus the most altered serum-specific mediator.
970 Expression ratios compare *Pkp2*$^{+/-}$ non-infected and *Pkp2*$^{+/-}$ MCMV to Ctr non-
971 infected, respectively; n = heart/serum: Ctr non-infected n = 10/10, *Pkp2*$^{+/-}$ non-
972 infected n = 10/10, Ctr MCMV n = 10/7, *Pkp2*$^{+/-}$ MCMV n = 10/8. **B+C**,
973 Representative gating and quantification of a myeloid-tailored flow cytometry panel of
974 cardiac CD45^{+} leukocytes from 6mpi hearts shown as absolute counts per milligram
975 tissue; Ctr non-infected n = 10, *Pkp2*$^{+/-}$ non-infected n = 8, Ctr MCMV n = 6, *Pkp2*$^{+/-}$
976 MCMV n = 8. Data are shown as mean ± SEM. Only male mice were used (square
977 symbol). Unpaired t test with or without Welch's correction or Mann-Whitney test, as
978 appropriate for 2 groups. Ordinary one-way ANOVA with or without Brown-Forsythe
979 and Welch's correction and Tukey's or Dunnett's T3 multiple comparisons,
980 respectively or Kruskal-Wallis test with Dunn's multiple comparisons, as appropriate
981 for >2 groups. Ctr – control, Neutro – neutrophils, Mo/Mac –
982 monocytes/macrophages, Mo – monocytes, Mac – macrophages.

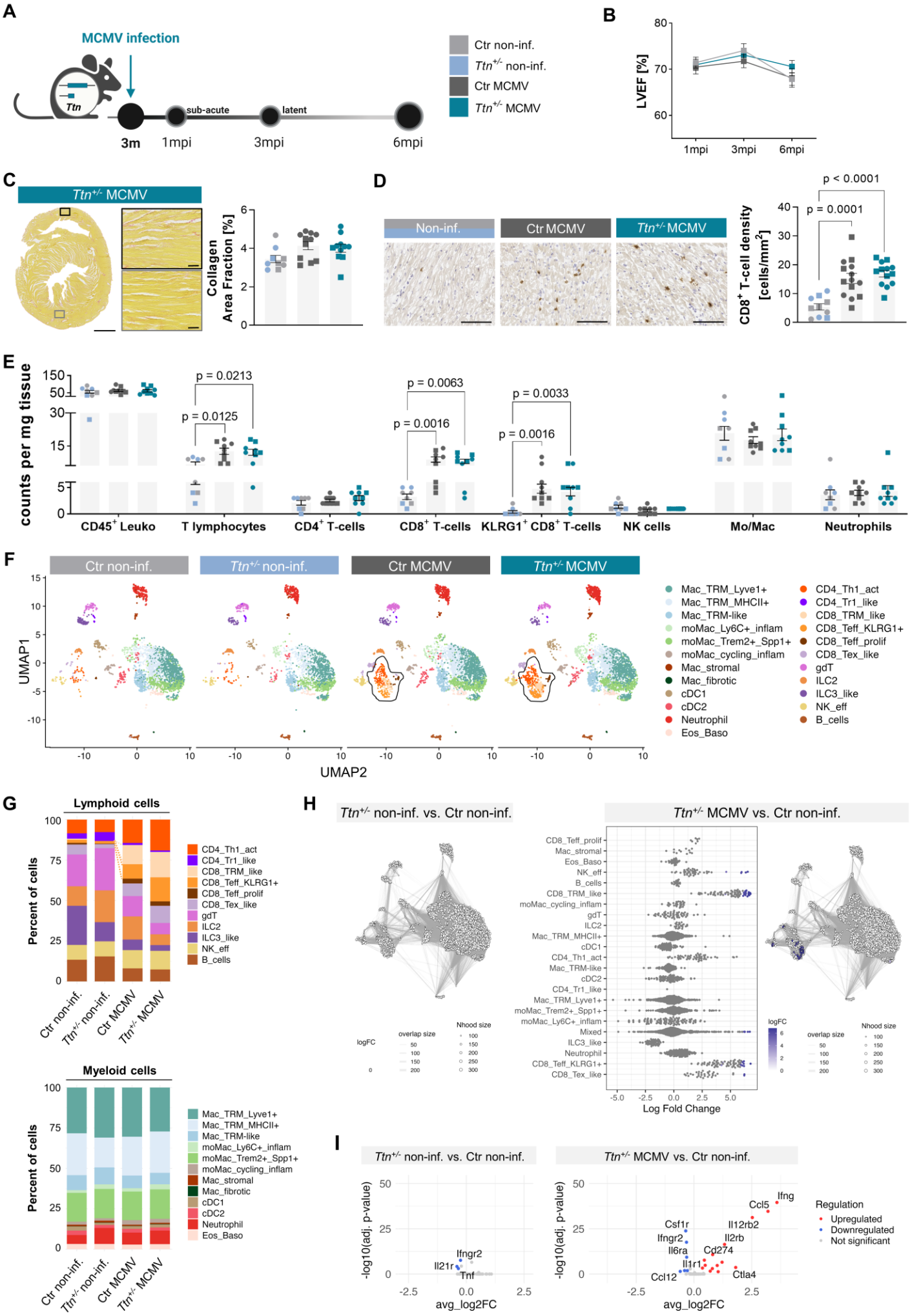
A
MCMV infection
Ttn
3m
1mpi
sub-acute
3mpi
latent
6mpi
Ctr non-inf.
Ttn+/- non-inf.
Ctr MCMV
Ttn+/- MCMV
B
LVEF [%]
80
70
60
1mpi
3mpi
6mpi
C
Ttn+/- MCMV
Collagen Area Fraction [%]
D
Non-inf.
Ctr MCMV
Ttn+/- MCMV
CD8+ T-cell density [cells/mm2]
p < 0.0001
p = 0.0001
E
counts per mg tissue
p = 0.0213
p = 0.0125
p = 0.0063
p = 0.0016
p = 0.0033
p = 0.0016
CD45+ Leuko
T lymphocytes
CD4+ T-cells
CD8+ T-cells
KLRG1+ CD8+ T-cells
NK cells
Mo/Mac
Neutrophils
F
Ctr non-inf.
Ttn+/- non-inf.
Ctr MCMV
Ttn+/- MCMV
UMAP1
UMAP2
Mac_TRM_Lyve1+
Mac_TRM_MHCII+
Mac_TRM-like
moMac_Ly6C+_inflam
moMac_Trem2+_Spp1+
moMac_cycling_inflam
Mac_stromal
Mac_fibrotic
cDC1
cDC2
Neutrophil
Eos_Baso
CD4_Th1_act
CD4_Tr1_like
CD8_TRM_like
CD8_Teff_KLRG1+
CD8_Teff_prolif
CD8_Tex_like
gdT
ILC2
ILC3_like
NK_eff
B_cells
G
Lymphoid cells
Percent of cells
Ctr non-inf.
Ttn+/- non-inf.
Ctr MCMV
Ttn+/- MCMV
Myeloid cells
H
Ttn+/- non-inf. vs. Ctr non-inf.
Ttn+/- MCMV vs. Ctr non-inf.
logFC
overlap size
Nhood size
Log Fold Change
I
Ttn+/- non-inf. vs. Ctr non-inf.
Ttn+/- MCMV vs. Ctr non-inf.
-log10(adj. p-value)
avg_log2FC
Ifngr2
Il21r
Tnf
Ifng
Ccl5
Csf1r
Il12rb2
Ifngr2
Il2rb
Il6ra
Cd274
Il1r1
Ccl12
Ctla4
Regulation
Upregulated
Downregulated
Not significant

Figure 5. MCMV does not trigger disease onset in a genetic mouse model of dilated cardiomyopathy with heterozygous loss of the sarcomeric gene *Ttn* (*Ttn*$^{+/-}$).

A, Schematic experimental design. 3-month-old *Ttn*$^{+/-}$ and control (Ctr) mice were infected with 5x10^5 plaque-forming units ∆m157-MCMV-eGFP (MCMV) or received phosphate-buffered saline (PBS) and were analyzed at different time points post-infection. Signature colors: Ctr non-infected (light grey), *Ttn*$^{+/-}$ non-infected (light blue), Ctr MCMV (dark grey) and *Ttn*$^{+/-}$ MCMV (blue). **B**, Left ventricular ejection fraction (LVEF) measured by echocardiography from 1 to 6 months post-infection (mpi); n = 1mpi/3mpi/6mpi: Ctr non-infected n = 5/5/4, *Ttn*$^{+/-}$ non-infected n = 5/5/5, Ctr MCMV n = 9/9/9, *Ttn*$^{+/-}$ MCMV n = 9/9/9. **C**, Representative picrosirius red stained *Ttn*$^{+/-}$ MCMV cardiac section and quantification of collagen area fraction at 6mpi; scale bars: overview 1000µm, detail 50 µm; Ctr non-infected + *Ttn*$^{+/-}$ non-infected n = 9, Ctr MCMV n = 11, *Ttn*$^{+/-}$ MCMV n = 11. **D**, Representative images of CD8$^+$ immunostaining in 6mpi heart sections and corresponding quantification of CD8$^+$ T-cell density; scale bar 50µm; Ctr non-infected + *Ttn*$^{+/-}$ non-infected n = 10, Ctr MCMV n = 14, *Ttn*$^{+/-}$ MCMV n = 13. **E**, Quantification of a lymphoid-tailored flow cytometry panel of cardiac CD45$^+$ leukocytes from 6mpi hearts shown as absolute counts per milligram tissue; Ctr non-infected + *Ttn*$^{+/-}$ non-infected n = 8, Ctr MCMV n = 9, *Ttn*$^{+/-}$ MCMV n = 9. **F**, UMAP representation of 12,660 cardiac leukocytes identified by CITE-seq split by experimental group at 6mpi; Ctr non-infected n = 2, *Ttn*$^{+/-}$ non-infected n = 2, Ctr MCMV n = 3, *Ttn*$^{+/-}$ MCMV n = 3. **G**, Relative cell type abundances across groups in lymphoid and myeloid cells at 6mpi. **H**, Assessment of statistically relevant changes in abundance using the MiloR package (p-value 0.1) in *Ttn*$^{+/-}$ non-infected and *Ttn*$^{+/-}$ MCMV versus Ctr non-infected, respectively. **I**, Comparative cytokine expression analysis in cardiac leukocytes (p-value 0.1) in *Ttn*$^{+/-}$ non-infected and *Ttn*$^{+/-}$ MCMV versus Ctr non-infected, respectively. Data are shown as mean ± SEM. Male: squares; female: circles. Ordinary one-way ANOVA with or without Brown-Forsythe and Welch's correction and Tukey's or Dunnett's T3 multiple comparisons, respectively or Kruskal-Wallis test with Dunn's multiple comparisons, as appropriate. Ctr – control, UMAP – uniform manifold approximation and projection, CITE-seq – cellular indexing of transcriptomes and epitopes by sequencing, NK cells – natural killer cells.

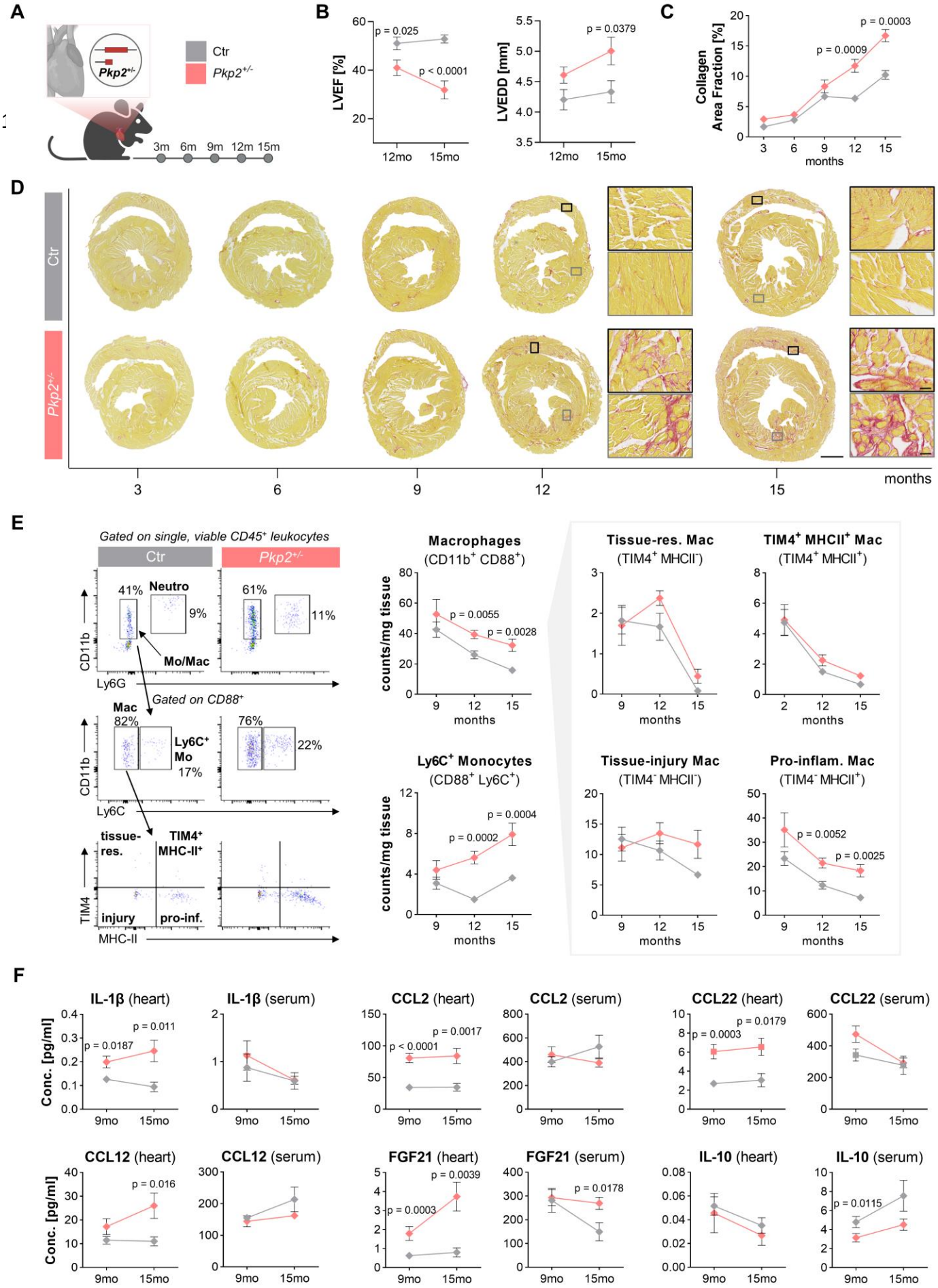
A
Pkp2+/-
Ctr
Pkp2+/-
3m 6m 9m 12m 15m
B
LVEF [%]
p = 0.025
p < 0.0001
12mo 15mo
LVEDD [mm]
p = 0.0379
12mo 15mo
C
Collagen Area Fraction [%]
p = 0.0003
p = 0.0009
months
D
Ctr
Pkp2+/-
3 6 9 12 15
months
E
Gated on single, viable CD45+ leukocytes
Ctr
Pkp2+/-
41% Neutro
9%
Mo/Mac
61%
11%
CD11b
Ly6G
Gated on CD88+
Mac 82%
Ly6C+ Mo 17%
76%
22%
Ly6C
tissue-res.
TIM4+ MHC-II+
injury
pro-inf.
TIM4
MHC-II
Macrophages (CD11b+ CD88+)
counts/mg tissue
p = 0.0055
p = 0.0028
months
Ly6C+ Monocytes (CD88+ Ly6C+)
p = 0.0004
p = 0.0002
Tissue-res. Mac (TIM4+ MHCII-)
TIM4+ MHCII+ Mac (TIM4+ MHCII+)
Tissue-injury Mac (TIM4- MHCII-)
Pro-inflam. Mac (TIM4- MHCII+)
p = 0.0052
p = 0.0025
F
IL-1β (heart)
p = 0.011
p = 0.0187
IL-1β (serum)
CCL2 (heart)
p = 0.0017
p < 0.0001
CCL2 (serum)
CCL22 (heart)
p = 0.0179
p = 0.0003
CCL22 (serum)
CCL12 (heart)
p = 0.016
CCL12 (serum)
FGF21 (heart)
p = 0.0039
p = 0.0003
FGF21 (serum)
p = 0.0178
IL-10 (heart)
IL-10 (serum)
p = 0.0115
Conc. [pg/ml]
9mo 15mo

Figure 6. Progressive development of a cardiac phenotype in aged *Pkp2*$^{+/-}$ mice.

A, Schematic overview of the experimental time points in *Pkp2*$^{+/-}$ and Ctr mice. **B**, Quantification of echocardiographic parameters at 12 and 15 months (mo); n = 12mo/15mo: Ctr n = 9/8, *Pkp2*$^{+/-}$ n = 9/9. **C+D**, Quantification of collagen area fraction and representative picrosirius red staining of cardiac sections from 3 to 15mo; scale bars: overview 1000µm, detail 50µm; n = 3mo/6mo/9mo/12mo/15mo: Ctr n = 4/7/12/6/7, *Pkp2*$^{+/-}$ n = 5/6/10/8/10. **E**, Representative gating and quantification of different cardiac CD45^{+} leukocytes at 9, 12 and 15mo by flow cytometry in counts per milligram tissue; n = 9mo/12mo/15mo: Ctr n = 11/6/12, *Pkp2*$^{+/-}$ n = 10/8/10. **F**, Cytokine profiling based on proximity extension assay at 9 and 15mo; n = 9mo/15mo: Ctr n = 10/6, *Pkp2*$^{+/-}$ n = 10/10. Data are shown as mean ± SEM. Unpaired t test with or without Welch's correction or Mann-Whitney test, as appropriate for 2 groups. Ordinary one-way ANOVA with or without Brown-Forsythe and Welch's correction and Tukey's or Dunnett's T3 multiple comparisons, respectively or Kruskal-Wallis test with Dunn's multiple comparisons, as appropriate for >2 groups. P-values for comparisons between groups at a given time point are shown in the graph; p-values for longitudinal comparisons within groups are provided in Table S14-S17. Ctr – control, LVEF – left ventricular ejection fraction, LVEDD – left ventricular end-diastolic diameter, Neutro – neutrophils, Mo/Mac – monocytes/macrophages, Mo – monocytes, Mac – macrophages.

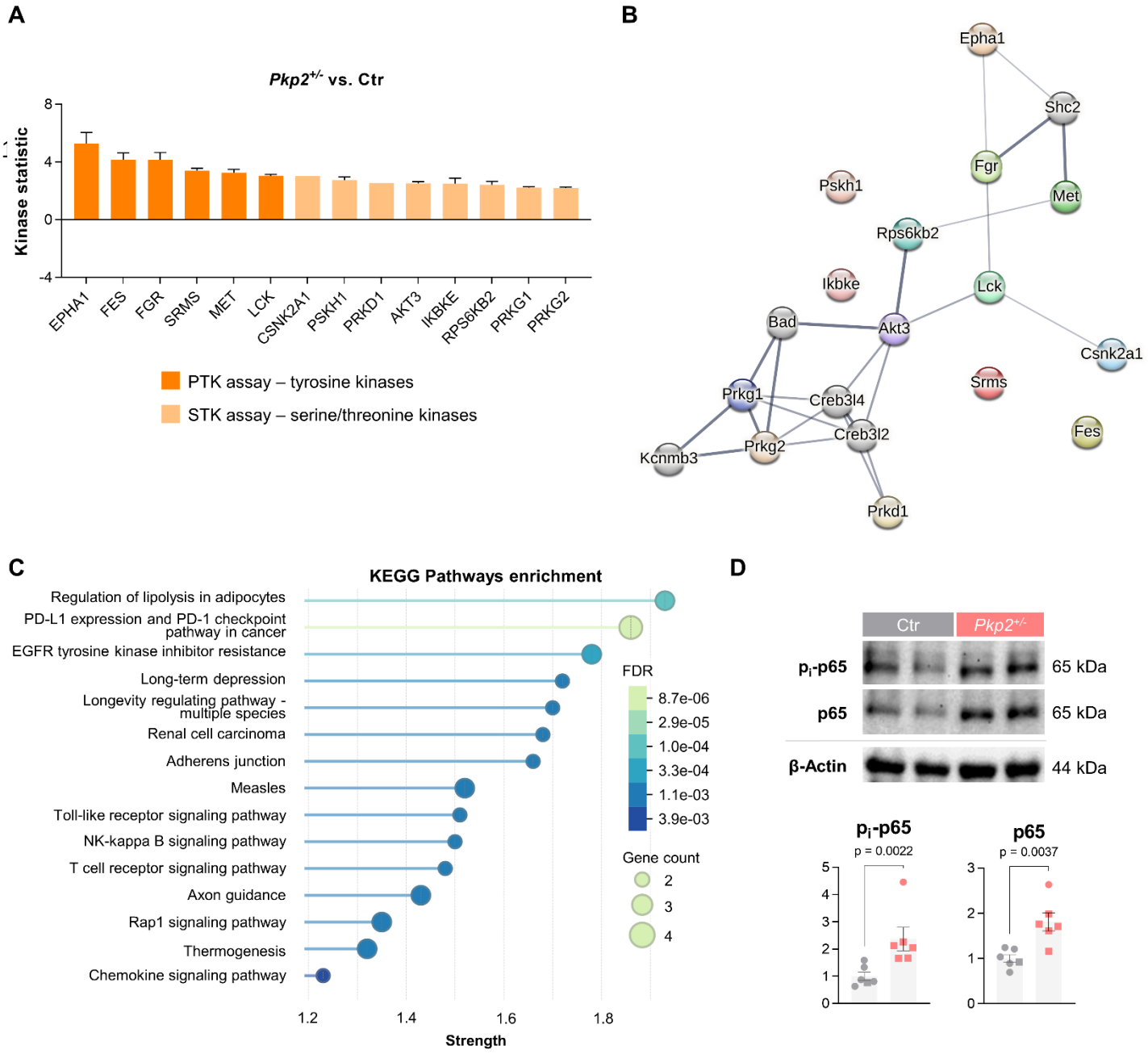
A
Pkp2+/- vs. Ctr
Kinase statistic
8
4
0
-4
EPHA1
FES
FGR
SRMS
MET
LCK
CSNK2A1
PSKH1
PRKD1
AKT3
IKBKE
RPS6KB2
PRKG1
PRKG2
PTK assay – tyrosine kinases
STK assay – serine/threonine kinases
B
Epha1
Shc2
Fgr
Met
Pskh1
Rps6kb2
Ikbke
Lck
Bad
Akt3
Csnk2a1
Srms
Prkg1
Creb3l4
Creb3l2
Fes
Kcnmb3
Prkg2
Prkd1
C
KEGG Pathways enrichment
Regulation of lipolysis in adipocytes
PD-L1 expression and PD-1 checkpoint pathway in cancer
EGFR tyrosine kinase inhibitor resistance
Long-term depression
Longevity regulating pathway - multiple species
Renal cell carcinoma
Adherens junction
Measles
Toll-like receptor signaling pathway
NK-kappa B signaling pathway
T cell receptor signaling pathway
Axon guidance
Rap1 signaling pathway
Thermogenesis
Chemokine signaling pathway
1.2
1.4
1.6
1.8
Strength
FDR
8.7e-06
2.9e-05
1.0e-04
3.3e-04
1.1e-03
3.9e-03
Gene count
2
3
4
D
Ctr
Pkp2+/-
pi-p65
65 kDa
p65
65 kDa
β-Actin
44 kDa
pi-p65
p = 0.0022
p65
p = 0.0037

1040 **Figure 7. Activation of inflammatory and compensatory signaling in *Pkp2*$^{+/-}$**
1041 **hearts at 12 months.**

1042 **A**, Comparative PamChip kinome profiling of *Pkp2*$^{+/-}$ hearts versus Ctr hearts at 12
1043 months; Ctr n = 4, *Pkp2*$^{+/-}$ n = 3. Bar plot representation of altered tyrosine (PTK) and
1044 serine/threonine (STK) kinases ranked by mean kinase statistic; Ctr n = 4, *Pkp2*$^{+/-}$ n =
1045 3. **B**, STRING interactions at medium confidence level. Line thickness correlates with
1046 predicted interaction strength. **C**, KEGG pathway enrichment of identified signaling
1047 networks. **D**, Western blot quantification and representative blot snips of
1048 phosphorylated p65 (p_i-p65, Ser536) and p65 protein levels in 15-month-old hearts
1049 normalized to β-Actin levels; Ctr n = 6, *Pkp2*$^{+/-}$ n = 6. Data are shown as mean ±
1050 SEM. Male: squares; female: circles. Unpaired t test with or without Welch's
1051 correction or Mann-Whitney test, as appropriate. Ctr – control, KEGG – Kyoto
1052 Encyclopedia of Genes and Genomes.

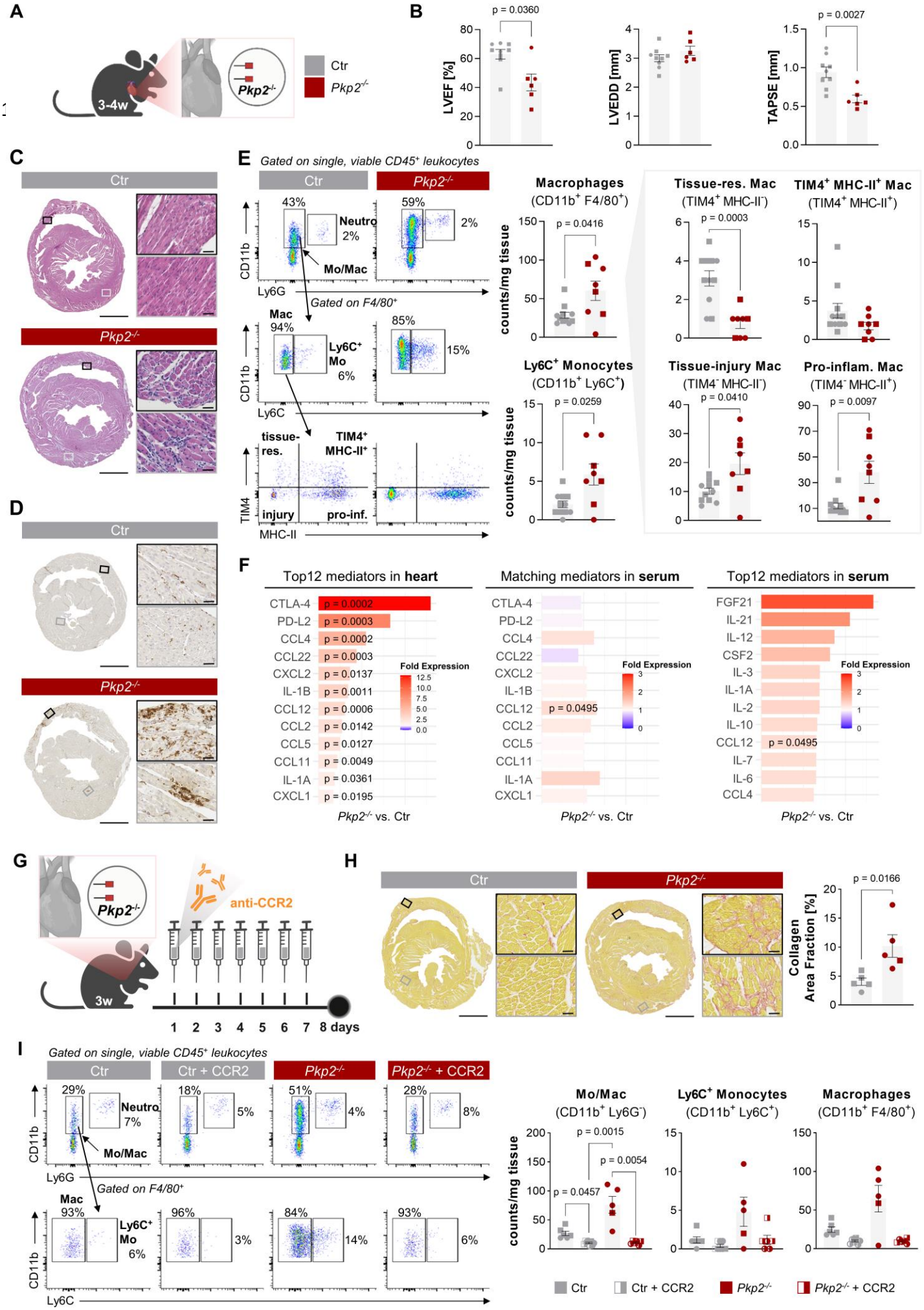
A
3-4w
Pkp2-/-
Ctr
Pkp2-/-
B
p = 0.0360
LVEF [%]
LVEDD [mm]
p = 0.0027
TAPSE [mm]
C
Ctr
Pkp2-/-
D
Ctr
Pkp2-/-
E
Gated on single, viable CD45+ leukocytes
Ctr
Pkp2-/-
43%
Neutro
2%
Mo/Mac
59%
2%
CD11b
Ly6G
Gated on F4/80+
Mac
94%
Ly6C+
Mo
6%
85%
15%
Ly6C
tissue-
res.
TIM4+
MHC-II+
injury
pro-inf.
TIM4
MHC-II
Macrophages
(CD11b+ F4/80+)
p = 0.0416
counts/mg tissue
Tissue-res. Mac
(TIM4+ MHC-II-)
p = 0.0003
TIM4+ MHC-II+ Mac
(TIM4+ MHC-II+)
Ly6C+ Monocytes
(CD11b+ Ly6C+)
p = 0.0259
Tissue-injury Mac
(TIM4- MHC-II-)
p = 0.0410
Pro-inflam. Mac
(TIM4- MHC-II+)
p = 0.0097
F
Top12 mediators in heart
CTLA-4 p = 0.0002
PD-L2 p = 0.0003
CCL4 p = 0.0002
CCL22 p = 0.0003
CXCL2 p = 0.0137
IL-1B p = 0.0011
CCL12 p = 0.0006
CCL2 p = 0.0142
CCL5 p = 0.0127
CCL11 p = 0.0049
IL-1A p = 0.0361
CXCL1 p = 0.0195
Fold Expression
Pkp2-/- vs. Ctr
Matching mediators in serum
CCL12 p = 0.0495
Top12 mediators in serum
FGF21
IL-21
IL-12
CSF2
IL-3
IL-1A
IL-2
IL-10
CCL12 p = 0.0495
IL-7
IL-6
CCL4
G
Pkp2-/-
anti-CCR2
3w
1 2 3 4 5 6 7 8 days
H
Ctr
Pkp2-/-
p = 0.0166
Collagen
Area Fraction [%]
I
Gated on single, viable CD45+ leukocytes
Ctr
Ctr + CCR2
Pkp2-/-
Pkp2-/- + CCR2
29%
Neutro
7%
Mo/Mac
18%
5%
51%
4%
28%
8%
Gated on F4/80+
Mac
93%
Ly6C+
Mo
6%
96%
3%
84%
14%
93%
6%
Mo/Mac
(CD11b+ Ly6G-)
p = 0.0015
p = 0.0054
p = 0.0457
Ly6C+ Monocytes
(CD11b+ Ly6C+)
Macrophages
(CD11b+ F4/80+)
counts/mg tissue
Ctr
Ctr + CCR2
Pkp2-/-
Pkp2-/- + CCR2

Figure 8 Anti-CCR2 intervention reduced numbers of recruited inflammatory monocytes and macrophages in more severely affected homozygous *Pkp2*$^{-/-}$ mice.

A, Schematic representation of homozygous cardiac-specific *Pkp2* knockout (*Pkp2*$^{-/-}$) mice at 3-4 weeks of age; signature colors: Ctr - grey, *Pkp2*$^{-/-}$ - dark red. **B**, Quantification of echocardiographic parameters at 3-4 weeks; Ctr n = 9, *Pkp2*$^{-/-}$ n = 6. **C**, Representative images of cardiac sections stained with hematoxylin-eosin (HE); scale bars: overview 1000µm, detail 50µm. **D**, Representative images of cardiac immunostaining against the macrophage surface marker CD68; scale bars: overview 1000µm, detail 50µm. **E**, Representative gating and quantification of different cardiac CD45^{+} leukocytes at 3-4 weeks by flow cytometry, shown in counts per milligram tissue; Ctr n = 11, *Pkp2*$^{-/-}$ n = 8. **F**, Cytokine profiling based on proximity extension assay at 3-4 weeks comparing expression ratios of *Pkp2*$^{-/-}$ versus Ctr heart and serum samples. Shown are the top 12 differentially expressed heart mediators with corresponding serum levels along with the top 12 most altered serum-specific mediators; n = heart/serum: Ctr n = 10/10, *Pkp2*$^{-/-}$ n = 10/10. **G**, Schematic representation of anti-CCR2 antibody treatment of *Pkp2*$^{-/-}$ and Ctr mice at 3 weeks of age. **H**, Representative picrosirius red staining of cardiac sections and quantification of collagen area fraction without anti-CCR2 treatment; scale bars: overview 1000µm, detail 50µm; Ctr n = 5, *Pkp2*$^{-/-}$ n = 5. **I**, Representative flow cytometry gating and quantification of different cardiac CD45^{+} leukocytes following anti-CCR2 treatment represented in counts per milligram tissue; untreated – filled symbol, anti-CCR2 treated – half-filled symbol; Ctr n = 6, Ctr+CCR2 n = 8, *Pkp2*$^{-/-}$ n = 5, *Pkp2*$^{-/-}$+CCR2 n = 6. Data are shown as mean ± SEM. Male: squares; female: circles. Unpaired t test with or without Welch's correction or Mann-Whitney test, as appropriate for 2 groups. Ordinary one-way ANOVA with or without Brown-Forsythe and Welch's correction and Tukey's or Dunnett's T3 multiple comparisons, respectively or Kruskal-Wallis test with Dunn's multiple comparisons, as appropriate for >2 groups. w – weeks, Ctr – control, LVEF – left ventricular ejection fraction, LVEDD – left ventricular end-diastolic diameter, TAPSE – tricuspid annular plane systolic excursion, Neutro – neutrophils, Mo/Mac – monocytes/macrophages, Mo – monocytes, Mac – macrophages.